Phase space conduits for reaction in multidimensional systems

Waalkens, Holger; Burbanks, Andrew; Wiggins, Stephen

Published in:
The Journal of Chemical Physics

DOI:
10.1063/1.1789891

Publication date:
2004

Phase space conduits for reaction in multidimensional systems: HCN isomerization in three dimensions

Holger Waalkens, Andrew Burbanks, and Stephen Wiggins
School of Mathematics, University of Bristol, University Walk, Bristol, BS8 1TW, United Kingdom

(Received 1 July 2004; accepted 16 July 2004)

The three-dimensional hydrogen cyanide/isocyanide isomerization problem is taken as an example to present a general theory for computing the phase space structures which govern classical reaction dynamics in systems with an *arbitrary* (finite) number of degrees of freedom. The theory, which is algorithmic in nature, comprises the construction of a dividing surface of minimal flux which is *locally* a ''surface of no return.'' The theory also allows for the computation of the global phase space transition pathways that trajectories must follow in order to react. The latter are enclosed by the stable and unstable manifolds of a so-called normally hyperbolic invariant manifold (NHIM). A detailed description of the geometrical structures and the resulting constraints on reaction dynamics is given, with particular emphasis on the three degrees of freedom case. A procedure is given which uses these structures to compute orbits homoclinic to, and heteroclinic between, NHIMs. The role of homoclinic and heteroclinic orbits in global recrossings of dividing surfaces and transport in complex systems is explained. The complete description provided here is inherently one within phase space; it cannot be inferred from a configuration space picture. A complexification of the classical phase space structures to incorporate quantum effects is also discussed. The results presented here call into question certain assumptions routinely made on the global dynamics; this paper provides methods that enable one to understand and quantify the phase space dynamics of reactions without making such assumptions.
[DOI: 10.1063/1.1789891]

I. INTRODUCTION

Transition state theory has a long and illustrious place in the field of chemistry, and in recent years its utility and applications have gone far beyond its origins. Following Truhlar,[1] ''transition state theory is the general name for any theory based in whole or in part on the fundamental assumption of transition state theory, or some quantum mechanical generalization of this assumption''; the ''fundamental assumption'' of the previous sentence is the existence of a hypersurface that (locally) divides phase space into two regions, corresponding to reactants and products. In what follows, we will refer to this hypersurface as the *dividing surface*. In order to be useful, the dividing surface should have certain properties that can be difficult to realize, in practice, and this has led to numerous versions of transition state theory. Inevitably, this leads to occasional confusion and ambiguity, with the situation being exacerbated by modern experimental techniques which reveal detailed real-time dynamical information about molecules as they undergo transitions from reactants to products. This is described vividly by Marcus[2]—''for a brief moment, the participants in the reaction may look like one large molecule ready to fall apart.'' The dividing surface, in addition to being a surface through which a trajectory passes during the reaction, represents a collection of possible dynamical states in its own right. This observation is amply born out in the rapidly developing experimental field known as transition state spectroscopy [see Ref. 3] which enables a direct *observation* of the ''the full family of configurations through which the reacting particles evolve *en route* from reagents to products.''

In this paper, we present a theory of *transition structures* that is firmly rooted in the dynamical arena of phase space. The geometrical picture we describe below has been formulated over the years in several works;[4–7] and we apply it to a well-known problem, HCN isomerization. For Hamiltonian systems with an *arbitrary* (but finite) number of degrees of freedom, the theory provides an algorithm for the *direct construction* of the transition structures which embody the dynamical features of the definition proposed by Polanyi and Zewail.[3] This includes the construction of a dividing surface which (locally) separates the energy surface into disjoint components, corresponding to reactants and products.

The dividing surface that we present is *locally* a ''surface of no return,'' i.e., it is free of locally recrossing trajectories whose presence would lead to an overestimation of reaction rates. In particular, this dividing surface can be shown to minimize the flux;[8] thus, it is the optimal dividing surface sought for in variational transition state theory, first proposed by Wigner,[9] with recent developments discussed in Refs. 10 and 11. For the computation of the flux, we provide an explicit formula that takes into account the full effect of nonlinearity and dynamics.

The construction of the dividing surface makes use of the existence of a so-called *normally hyperbolic invariant manifold* (NHIM) (Ref. 12), which can be shown to exist near equilibrium points of saddle-center-...-center stability type. Such equilibria are characteristic of most kinds of ''re-

action type'' dynamics in a large and diverse number of applications in chemistry and physics, as we will explain below in more detail. Normal hyperbolicity means that the rates of contraction and expansion for the invariant motion on the NHIM are dominated by those in the directions transverse to the NHIM. It is this property of the NHIM which largely governs the dynamics nearby. The NHIM can be identified with the energy surface of the so-called ''activated complex'' (see the orginal work by Eyring[13] and, e.g., Miller[14] for a more recent perspective) which, as an unstable invariant ''supermolecule,''[15] is located between reactants and products.

It is useful to point out that there is some confusion in terminology in the literature concerning the notion of *transition state*: this term is sometimes used to refer to the dividing surface through which reacting trajectories pass, and sometimes to the activated complex, which is mathematically realized by the NHIM, and through which trajectories *never* pass. In the latter case, where the phrase ''crosses the transition state'' appears in the literature, it actually refers to trajectories crossing the *projection of the* NHIM *into configuration space*; trajectories cannot cross the NHIM (in phase space) because it is an invariant manifold. For clarity, in what follows, we will refer explicitly to the *dividing surface* (through which reacting trajectories pass) and the NHIM (which is an *invariant manifold*), and will spare confusion by avoiding use of the term ''transition state.''

In the above, we have talked of transition *structures* in order to emphasize that we not only construct a dividing surface with the desired properties, but we also construct the conduits in phase space that reacting trajectories must follow. In fact, the NHIM has stable and unstable manifolds which are of one less dimension than the energy surface; they act as separatrices, enclosing the energy surface volumes which contain all reacting trajectories; all nonreacting trajectories are contained in the complement of these volumes. The transition structures thus carry with them an intrinsic set of reaction coordinates that provides an exact *dynamical* road map of the energy surface. The regions of the energy surface within which reacting trajectories start, and the regions into which they pass, can thus be determined. This is of central importance for questions of state-specific reactivity (see Refs. 16 and 17), and control of reactivity (see Refs. 18 and 19).

Moreover, we describe a procedure to compute intersections of the stable and unstable manifolds of the same, or different, NHIMs. Intersections of stable and unstable manifolds of the same NHIM provide a mechanism for ''global'' recrossings of the dividing surface, i.e., a mechanism by which a trajectory that has crossed the dividing surface, and has left the neighborhood of the dividing surface, may reapproach the dividing surface and possibly cross it again. The intersections of the stable and unstable manifolds of NHIMs that correspond to different equilibrium points provide a skeleton that trajectories may follow in order to find their way through a succession of dividing surfaces. This is of fundamental importance in the study of so-called *rare events* in many complex systems, in which several saddle-center-...-center equilibria coexist.[20]

It is worth mentioning that the theory that we present is not restricted to Hamiltonians of the type ''kinetic plus potential energy,'' i.e., it also applies to Hamiltonians which contain magnetic or Coriolis terms due to rotations. Moreover, it is important to emphasize that our transition structures, which contain the complete information about the transition geometry and dynamics, are inherently *phase space* objects. The complete information which these structures embody cannot be obtained from theories which are based on a *configuration space* picture.

In the spirit of classical transition state theory we set out our theory in the framework of classical mechanics. However, the geometry of the transition structures in classical phase space, and their complexification, provides a natural setting for the study of quantum effects, as we will describe.

This paper consists of two main parts: Sec. II which contains a detailed description of the general theory and Sec. III in which the theory is applied to the HCN/CNH isomerization problem. These main parts are organized as follows. In Sec. II A we stress the importance of saddle-center-...-center equilibrium points, or ''saddles'' for short, in diverse applications. Section II B introduces the phase space structures which can be shown to exist near saddles and which control the transport ''across'' saddles. In Sec. II C we consider the dynamics in the neighborhood of a saddle, which—provided a generic nonresonance condition is fulfilled—is integrable, and we describe the dynamics in terms of *normal form coordinates*. In the neighborhood of a saddle the normal form coordinates give explicit expressions for the phase space structures which control the transport. These are discussed in detail in Sec. II D. In Sec. II E we explain how the local phase space structures can be ''globalized,'' i.e., continued out of the neighborhood of the saddle. An exact formula for the flux ''across'' the saddle is given in Sec. II F. Quantum effects are addressed in Sec. II G. In Sec. III we show the results of the computation of the various phase structures introduced in Sec. II for the three-degrees-of-freedom HCN/CNH isomerization problem. This includes the computation and discussion of a *dynamical reaction path* which we compare with the so-called minimum energy path in Sec. III A. Global aspects of HCN/CNH isomerization are contained in Secs. III B and III C, in which we discuss how initial conditions of reactive trajectories can be found in the HCN potential well, and also explain the role of homoclinic and heteroclinic orbits in questions of global recrossings and crossings of multiple dividing surfaces. Certain homoclinic orbits allow us to infer the existence of a high-dimensional chaotic saddle, which we discuss in Sec. III D. Conclusions are given in Sec. IV.

II. THE CLASS OF SYSTEMS OF INTEREST

We begin in the realm of classical mechanics, with a Hamiltonian function describing a system of interest. The Hamiltonian may be expressed in any convenient set of coordinates, may have any number n degrees of freedom (DOF), and does *not* have to be of the form ''kinetic plus potential energy,'' e.g., it can include rotational or magnetic terms.

A. Saddle points

The appropriate phase space structures are associated with equilibrium points, of Hamilton's equations for the system, that are of a certain type. Namely, the matrix associated with the linearization of Hamilton's equations about the equilibrium point has a pair of real eigenvalues of opposite signs ($\pm\lambda$) and $2n-2$ purely imaginary eigenvalues, occurring in complex conjugate pairs ($\pm i\omega_j, j=2,...,n$). Such equilibria are called saddle-center-...-centers. Structures associated with this type of equilibrium point provide the fundamental mechanism for ''transformation'' (or ''reaction'') in a large, and diverse, number of applications, in which their *dynamical* consequences have largely remained a mystery. For example, in condensed matter physics, this mechanism was described as much as 20 years ago, in the context of the development of a rate theory for the migration of atoms in solids.[21] More recently, such saddles have been shown to play a key role in the study of the ''landscape paradigm.''[22] The landscape paradigm is central to the study of many complex systems, including glasses and biomolecules, but no tools have been introduced to study the complex deterministic dynamics of the resulting Hamiltonian systems. In cosmology, it was recently shown that orbits related to a saddle-center-center, in a general Bianchi-type IX model, appear to be the mechanism giving rise to chaos.[23] A problem of much current interest in chemistry concerns the dissociation rates of ozone, which are still a mystery, where agreement with experimental results can only be obtained by making certain assumptions on the dynamics (see the discussion of non-Rice-Ramsperger-Kassel-Marcus behavior in Refs. 24 and 25). This problem fits exactly into the framework we are developing here. For energies of interest, ozone can dissociate from its so-called ''open minima'' through two exits,[26] which both contain barriers associated with equilibria of saddle-center-center type. Of course, saddle-center-center equilibria have played a key role in questions related to capture and escape in celestial mechanics for many years: The Lagrange points L_1 and L_2, of the circular restricted three-body problem, are examples of such saddles. Recently, a transition state theory approach has been applied in that setting to study the capture probability by the Earth of debris ejected from Mars as a result of asteroid impacts.[27] These examples highlight not just the ubiquity of the saddle-center-...-center type equilibrium point as a dynamical mechanism for transformation in phase space, but also the broad applicability of the transition state theory approach, far beyond its original place of conception in chemistry.

Locating saddles is in the spirit of classical transition state theory, but there is an important difference here. We are concerned with the *dynamical consequences* of certain types of saddles of Hamilton's equations in phase space. The usual approach is to consider saddles of the potential energy surface (the setting of the ''landscape paradigm''). Of course, if the Hamiltonian has the form of the sum of a kinetic energy term and a potential energy term, then there is a correspondence between the saddles of the potential energy surface and the saddle type equilibria of Hamilton's equations. Here, however, we emphasize the influence of this saddle in the dynamical arena of phase space. A central point is that it is difficult, and often misleading, to try to infer dynamics from properties of configuration space. In reinforcing this point, we begin by considering the geometry of the energy surface near such saddle-center-...-center equilibrium points (henceforth referred to simply as ''saddles'') in phase space.

B. The dividing surface, the NHIM, and its stable and unstable manifolds

For energies above that of the saddle, the $(2n-1)$-dimensional energy surface has locally the structure of the product of a $(2n-2)$-dimensional sphere with an interval, $S^{2n-2}\times I$. It will turn out that I corresponds to a natural, dynamical, ''reaction coordinate'' in phase space, and S^{2n-2} will correspond to bath modes, or vibrations ''normal'' to the reaction coordinate. Now it follows, from work in Refs. 4–7, that on these energy surfaces, and ''close enough'' to the saddle (where ''closeness'' is a problem-dependent quality that must be determined numerically), there exists a $(2n-2)$-dimensional sphere, S^{2n-2}, which is our *dividing surface*. The $(2n-2)$-dimensional sphere has an ''equator'': a $(2n-3)$-sphere S^{2n-3}, which separates the dividing surface into two halves, corresponding to forward and backward reactions. Except for the equator (which is an invariant manifold), the dividing surface is locally a ''surface of no return,'' in the sense that trajectories that cross the dividing surface in the energy surface must exit the neighborhood of the dividing surface before they can possibly cross it again. Most importantly, for reaction dynamics, the dividing surface has the ''bottleneck property.'' This means that it locally divides the energy surface into two disjoint components, which correspond to reactants and products. The *only* way a trajectory can pass from one component of the energy surface to the other is to pass through the dividing surface. The issue of ''recrossing'' is an important part of the choice of the dividing surface. Truhlar[1] distinguishes two types of recrossing: local and global recrossing. Local recrossing cannot occur with our choice of dividing surface. However, global recrossing is a very different matter. We will show that the existence of homoclinic orbits and heteroclinic cycles is an intrinsic feature of the dynamics. Their existence implies that global recrossing *cannot* be avoided, regardless of the choice of dividing surface; in other words, global recrossing is a fundamental property of the dynamics; its presence does not, therefore, indicate the limitations of any particular method for constructing a dividing surface. Homoclinic and heteroclinic orbits are responsible for long time correlations in the dynamics and chaos, which we will describe in more detail shortly.

During the rapid growth period of nonlinear dynamics in the 1970s and 1980s, much work was done on applying ideas from dynamical systems theory to chemical reaction dynamics in two DOF systems. Variational transition state theory deals with the local recrossing problem by varying the dividing surface, so that the flux across it is minimized. Fundamental work was done by Pechukas and co-workers,[28,29] in developing a transition state theory for two DOF systems. In the three-dimensional (3D) energy surface, they showed that, under certain conditions, a periodic orbit can be found that bounds a 2D surface in phase space which is a ''surface of no

return'' across which the flux is minimal. The question of how to generalize this to n DOF systems with $n \geqslant 3$ is answered by our definition and construction of the dividing surface: our dividing surface is a $(2n-2)$ sphere which has one dimension less than the energy surface. It separates reactants from products and is transverse to the Hamiltonian flow, i.e., it is a surface of no return, except for an invariant $(2n-3)$ sphere which, as its equator, divides it into forward- and backward-reactive hemispheres. The flux for this dividing surface is minimal, in a sense that is made mathematically precise in Ref. 8. Substituting $n=2$ into our formulas, we recover exactly the results by Pechukas and co-workers;[28,29] for two DOF the NHIM is a single Lyapunov periodic orbit, which is the periodic orbit appearing in their theory. It is in this sense that conventional transition state theory and variational transition state theory merge. This is discussed in detail in Ref. 8, where also some confusing points in the literature are clarified. For two DOF systems, the PODS theory is more general than the theory that we present, in that it can be applied to a larger class of periodic orbits, including those that result from bifurcations of the Lyapunov periodic orbit. However, it is equally important to realize that periodic orbits lack sufficient dimensionality to be useful for constructing dividing surfaces for systems with three or more DOF. Although the theory that we present is applicable to such systems, the study of *bifurcations* of NHIMs has yet to be extended to the general DOF case.

It is important to understand that there is a strong geometrical constraint on how trajectories may cross the dividing surface. The two halves of the dividing surface correspond to forward and backward reactions. The equator is an invariant $(2n-3)$-dimensional sphere S^{2n-3} of saddle stability type. More precisely, it is a *normally hyperbolic invariant manifold* (NHIM) (Ref. 12), which means that the expansion and contraction rates of the dynamics on the $(2n-3)$ sphere are dominated by those transverse to it. As will be explained in more detail below, the NHIM is the energy surface of an unstable invariant subsystem with one DOF less than the full system. This subsystem is what, in the chemical literature, is referred to as an ''activated complex.''[13,14] The theory of normally hyperbolic invariant manifolds provides a mathematical proof of the existence of this unstable ''supermolecule,''[15] located between reactants and products, as mentioned in the Introduction. Just like a saddle point, the NHIM has stable and unstable manifolds. In this case, the stable and unstable manifolds are $(2n-2)$ dimensional, having the structure of *spherical cylinders*, $S^{2n-3}\times\mathbb{R}$. It is most significant that they are of one less dimension than the energy surface and can therefore act as ''separatrices,'' i.e., they enclose volumes of the energy surface. Their key dynamical significance is that the only way that trajectories can pass through the dividing surface (and thereby react) is if they are in certain volumes enclosed by the stable and unstable spherical cylinders.

Thus far, our description has been of the geometry near the dividing surface. However, the stable and unstable spherical cylinders can exist ''far'' from the dividing surface, ''snaking'' their way through phase space. This is significant because they bound certain volumes in phase space consisting of trajectories that react by passing through this dividing surface. Moreover, as we make clear below, these spherical cylinders bound the true ''phase space reaction paths.'' The ability to compute these manifolds, and to track them far away from the transition region, is the key to the study of state-specific reactivity,[16,17] of dynamical effects on reactions[30,31] of control of reactivity[18,19] and as will be discussed below in more detail, of rare events.[20]

C. Phase space dynamics near the dividing surface

In a neighborhood of the saddle, the phase space geometry, described above, can be realized through a special set of coordinates, in which many of the desired features of transition state theory become transparent. These coordinates can be constructed in an algorithmic fashion, using the well-known Poincaré-Birkhoff normalization procedure. Most importantly, this procedure also yields the canonical transformation between the original coordinates (whatever they may be) and the *normal form coordinates*. In the normal form coordinates, the dividing surface, the NHIM, and its stable and unstable manifolds, can be expressed by explicit equations. In this way, the relationship between the local phase space geometry and reacting and nonreacting trajectories can be completely understood. The geometrical structures and trajectories can then be transformed back into the original coordinate system by the inverse of the normal form transformation.

More precisely, in a neighborhood of the saddle, a special set of coordinates is constructed, denoted $(q_1,\ldots,q_n,p_1,\ldots,p_n)$. In these coordinates, it can be verified easily that the function $\mathcal{I}=q_1p_1$ is an integral of the motion (i.e., it is constant on trajectories) and, if the numbers ω_j, $j=2,\ldots,n$, satisfy a (generic) nonresonance condition, then the quantities $J_i=(p_i^2+q_i^2)/2$, $i=2,\ldots,n$, are also integrals of the motion, The Hamiltonian can then be written solely as a function of these integrals, i.e., $H_{\mathrm{NF}}=H_{\mathrm{NF}}(\mathcal{I},J_2,\ldots,J_n)$. In this coordinate system, Hamilton's equations take the following simple form:

$$
\begin{aligned}
\dot{q}_1 &= \frac{\partial H_{\mathrm{NF}}}{\partial \mathcal{I}}(\mathcal{I},J_2,\ldots,J_n)q_1,\\
\dot{p}_1 &= -\frac{\partial H_{\mathrm{NF}}}{\partial \mathcal{I}}(\mathcal{I},J_2,\ldots,J_n)p_1,\\
\dot{q}_i &= \frac{\partial H_{\mathrm{NF}}}{\partial J_i}(\mathcal{I},J_2,\ldots,J_n)p_i,\\
\dot{p}_i &= -\frac{\partial H_{\mathrm{NF}}}{\partial J_i}(\mathcal{I},J_2,\ldots,J_n)q_i, \quad i=2,\ldots,n.
\end{aligned}
\tag{1}
$$

This is significant, because the coefficients in these equations are constant on trajectories (since they are functions only of the integrals). Therefore, Hamilton's equations separate near the saddle, and can also be trivially integrated. The bath modes, or ''internal coordinates'' [described by $(q_2,\ldots,q_n,p_2,\ldots,p_n)$], separate from the reaction coordinates [described by (q_1,p_1)]. This puts on a rigorous mathematical and algorithmic foundation discoveries showing

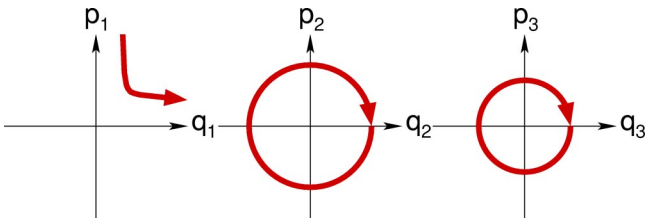

FIG. 1. Projection of a typical trajectory to the plane of the reaction coordinates (q_1,p_1) and to the planes of the bath modes (q_i,p_i), $i=2,...,n$, for $n=3$ DOF. The arrows mark the direction of time.

regularity in complex reaction paths by Hinde and Berry,[32] Komatsuzaki and Berry,[33] which were anticipated early on by Miller,[34] and further carried out by Hernandez and Miller,[35] which suggested that the decoupling of the reaction degree-of-freedom from the bath was a general phenomenon. This work goes further by showing that, under generic conditions, the normal form, describing the original system in a neighborhood of the dividing surface, is integrable up to arbitrarily high degree. Note that it is not "separable" in the classical sense that this term is used, but, since the coefficients of Eq. (1) are constant on trajectories, the system does separate into n decoupled systems: a saddle, and $n-1$ oscillators. Figure 1 shows the projections of a typical trajectory to the various normal form coordinate planes. Due to the constant nature of the integrals, the trajectory projects to circles $(p_i^2+q_i^2)/2=J_i$ in the bath coordinate planes (q_i,p_i), $i=2,...,n$, and to an hyperbola in the plane of the reaction coordinates (q_1,p_1). The J_i, $i=2,...,n$, are the actions $\oint p_i dq_i/(2\pi)$ of the bath modes and, as we will see below in more detail, the saddle integral $\mathcal{I}$ has the natural interpretation of being the action of a complex tunnelling path.

The coefficients, $\partial H_{\mathrm{NF}}(\mathcal{I},J_2,\ldots,J_n)/\partial J_i$, $i=2,...,n$, in the equations of motion (1), are the "normal frequencies," which contain the full effect of nonlinearity. This provides a very natural way to study resonances amongst the internal coordinates for motions near the dividing surface.

D. Local transition structures in the normal form coordinates

In the following, we show how the normal form, which is valid in the neighborhood of the saddle, gives *explicit formulas* for the various manifolds mentioned in Sec. II B. Many of these structures are discussed in detail in Ref. 7. The pictures are for three DOF. In fact, conceptually, the step from two to three DOF is the big step; once the case of three DOF is well understood, it is not difficult to incorporate more DOF. We begin by describing the local structure of the energy surfaces.

1. Energy surfaces

For $E<0$, the energy surface consists of two disjoint components, each having the structure of a "spherical cone," where a spherical cone is a family of $(2n-2)$ spheres S^{2n-2} that is parametrized along an interval such that the $(2n-2)$ spheres shrink to a point at one end of the interval. The two components correspond to "reactants" and "products." The top panel of Fig. 2 shows how the spherical cones

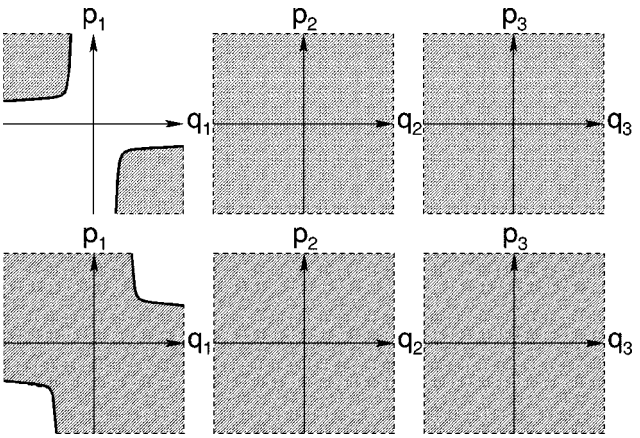

FIG. 2. Projection of energy surfaces (shaded regions) to the planes of the normal form coordinates. The energy surface in the top panel has $E<0$; the energy surface in the bottom panel has $E>0$.

project to the various planes of the normal form coordinates. The projection to the plane of the reaction coordinates (q_1,p_1) is bounded away from the origin by two hyperbolas, $q_1p_1=\mathcal{I}<0$, where $\mathcal{I}$ is given implicitly by the energy equation with the bath actions J_i, $i=2,...,n$, set equal to zero: $H_{\mathrm{NF}}(\mathcal{I},0,...,0)=E<0$. The projections to the planes of the bath coordinates, (q_i,p_i), $i=2,...,n$, are unbounded.

At $E=0$, the formerly disconnected components merge (the energy surface bifurcates), and for $E>0$ the energy surface has locally the structure of a spherical cylinder, $S^{2n-2}\times I$. Its projection to the plane of the reaction coordinates now includes the origin. In the first and third quadrants it is bounded by two hyperbolas, $q_1p_1=\mathcal{I}>0$, where $\mathcal{I}$ is again given implicitly by the energy equation with all bath actions equal to zero, but now with a positive energy: $H_{\mathrm{NF}}(\mathcal{I},0,...,0)=E>0$. The projections to the planes of the bath coordinates are again unbounded. The bottom panel of Fig. 2 illustrates this.

2. The dividing surface and reacting and nonreacting trajectories

On an energy surface with $E>0$, we define the dividing surface by $q_1=p_1$. This gives a $(2n-2)$ sphere which we denote by $S_{ds}^{2n-2}(E)$. Its projection to the reaction coordinates simply gives a line segment through the origin which joins the boundaries of the projection of the energy surface, as shown in Fig. 3. The projections of the dividing surface to the planes of the bath coordinates are bounded by circles $(p_i^2+q_i^2)/2=J_i$, $i=2,...,n$, where J_i is determined by the energy equation with the other bath actions, J_k, $k\neq i$, and the saddle integral, $\mathcal{I}$, set equal to zero. The dividing surface divides the energy surface into two halves, $p_1-q_1>0$ and $p_1-q_1<0$, corresponding to reactants and products.

As mentioned in Sec. II C, trajectories project to hyperbolas in the plane of the reaction coordinates, and to circles in the planes of the bath coordinates. The sign of $\mathcal{I}$ determines whether a trajectory is nonreacting or reacting, see Fig. 3. A trajectory which has $\mathcal{I}<0$ stays on the reactant or product side; a trajectory with $\mathcal{I}>0$ either reacts in the forward direction, i.e., from reactants to products, or in the

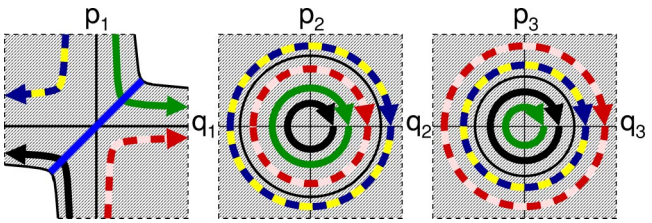

FIG. 3. Projection of the dividing surface and reacting and nonreacting trajectories to the planes of the normal form coordinates. In the plane of the reaction coordinates, the projection of the dividing surface is the bold diagonal line segment, which has $q_1=p_1$. In the planes of the bath coordinates, the projections of the dividing surface are the disks bounded by the thin circles. Forward and backward reactive trajectories (bold curves) project to the first and third quadrant in the plane of the reaction coordinates, respectively, and pass through the dividing surface. The dashed curves mark nonreactive trajectories on the reactant side ($p_1-q_1>0$), and on the product side ($p_1-q_1<0$), of the dividing surface. The shaded regions indicate the projections of the energy surface.

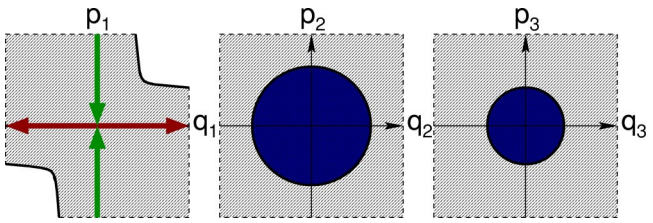

FIG. 4. The projection of the NHIM and the local parts of its stable and unstable manifolds, $W^s(E)$ and $W^u(E)$, to the planes of the normal form coordinates. In the plane of the reaction coordinates, the projection of the NHIM is the origin, and the projection of $W^s(E)$ and $W^u(E)$ are the p_1 axis and q_1 axis, respectively. $W^s(E)$ consists of the forward and backward branches $W_f^s(E)$ and $W_b^s(E)$, which have $p_1>0$ and $p_1<0$, respectively; $W^u(E)$ consists of $W_f^u(E)$ and $W_b^u(E)$, which have $q_1>0$ and $q_1<0$, respectively. In the plane of the bath coordinates, the projections of the NHIM, $W^s(E)$, and $W^u(E)$ (the darkly shaded circular discs) coincide with the projection of the dividing surface in Fig. 3. The lightly shaded regions mark the projections of the energy surface.

backward direction, i.e., from products to reactants. While the projections of reactive trajectories to the planes of the *bath* coordinates are always contained in the projections of the dividing surface. In this, and other ways, the geometry of the reaction is highly constrained. There is no analogous restriction on the projections of nonreactive trajectories to the bath coordinates.

3. The NHIM, its stable and unstable manifolds, and its fibration by invariant tori

On an energy surface with $E>0$, the NHIM is given by $q_1=p_1=0$. The NHIM has the structure of a $(2n-3)$ sphere, which we denote by $S^{2n-3}_{\mathrm{NHIM}}(E)$. The NHIM is the equator of the dividing surface; it divides it into two ''hemispheres'': the *forward dividing surface*, which has $q_1=p_1>0$, and the *backward dividing surface*, which has $q_1=p_1<0$. The forward and backward dividing surfaces have the structure of $(2n-2)$-dimensional balls, which we denote by $B^{2n-2}_{ds,f}(E)$ and $B^{2n-2}_{ds,b}(E)$, respectively. All forward reactive trajectories cross $B^{2n-2}_{ds,f}(E)$; all backward reactive trajectories cross $B^{2n-2}_{ds,b}(E)$. Since $q_1=p_1=0$ in the equations of motion (1) implies that $\dot{q}_1=\dot{p}_1=0$, the NHIM is an invariant manifold, i.e., trajectories started in the NHIM stay in the NHIM for all time. The system resulting from $q_1=p_1=0$ is an invariant subsystem with one DOF less than the full system. This is the ''activated complex,'' located between reactants and products (see Sec. II B). The NHIM can be considered to be the energy surface of the activated complex. In particular, all trajectories in the NHIM have $\mathcal{I}=0$.

The equations of motion (1) also show that $\dot{p}_1-\dot{q}_1<0$ on the forward dividing surface $B^{2n-2}_{ds,f}(E)$, and $\dot{p}_1-\dot{q}_1>0$ on the backward dividing surface $B^{2n-2}_{ds,b}(E)$. Hence, except for the NHIM, which is an invariant manifold, the dividing surface is everywhere transverse to the Hamiltonian flow. This means that a trajectory, after having crossed the forward or backward dividing surface, $B^{2n-2}_{ds,f}(E)$ or $B^{2n-2}_{ds,b}(E)$, respectively, must leave the neighborhood of the dividing surface before it can possibly cross it again, i.e., the dividing surface is *locally* a ''surface of no return.'' Indeed, such a trajectory must leave the local region in which the normal form is valid before it can possibly cross the dividing surface again.

Since the NHIM is of saddle stability type, it has stable and unstable manifolds, $W^s(E)$ and $W^u(E)$. The stable and unstable manifolds have the structure of spherical cylinders, $S^{2n-3}\times\mathbb{R}$. Each of them consists of two branches: the ''forward branches,'' which we denote by $W_f^s(E)$ and $W_f^u(E)$, and the ''backward branches,'' which we denote by $W_b^s(E)$ and $W_b^u(E)$. In terms of the normal form coordinates, $W_f^s(E)$ is given by $q_1=0$ with $p_1>0$, $W_f^u(E)$ is given by $p_1=0$ with $q_1>0$, $W_b^s(E)$ is given by $q_1=0$ with $p_1<0$, and $W_b^u(E)$ is given by $p_1=0$ with $q_1<0$, see Fig. 4. Trajectories on these manifolds have $\mathcal{I}=0$.

The NHIM has a special structure: Due to the conservation of the bath actions, it is filled, or *foliated*, by invariant $(n-1)$-dimensional tori, T^{n-1}. More precisely, for $n=3$, each value of J_2 implicitly defines a value of J_3 by the energy equation $H_{\mathrm{NF}}(0,J_2,J_3)=E$. For three DOF, the NHIM is thus foliated by a one-parameter family of invariant 2-tori. The end points of the parametrization interval correspond to $J_2=0$ (implying $q_2=p_2=0$) and $J_3=0$ (implying $q_3=p_3=0$), respectively. At the end points, the 2-tori thus degenerate to periodic orbits, the so-called *Lyapunov periodic orbits*. This foliation of $S^3_{\mathrm{NHIM}}(E)$ is the so-called *Hopf fibration*. As we will discuss below in more detail, the fact that the NHIM is foliated by invariant tori has consequences for the corresponding quantum system.

4. Forward and backward reaction paths

Since the stable and unstable manifolds of the NHIM are of one less dimension than the energy surface, they enclose volumes of the energy surface. We call the union of the forward branches, $W_f^s(E)$ and $W_f^u(E)$, the *forward reactive spherical cylinder* and denote it by $W_f(E)$. Similarly, we define the *backward reactive spherical cylinder* $W_b(E)$ as the union of the backward branches, $W_b^s(E)$ and $W_b^u(E)$.

The reactive volumes enclosed by $W_f(E)$ and $W_b(E)$ are shown in Fig. 5 as their projections to the normal form coordinate planes. In the plane of the reaction coordinates, the

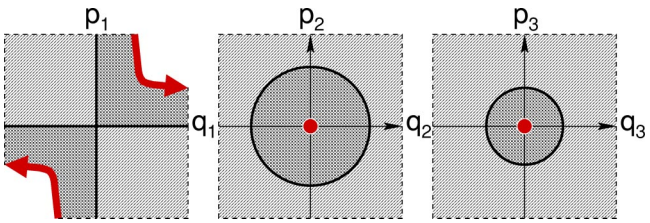

FIG. 5. Projections of the reactive volumes enclosed by the forward and backward reactive spherical cylinders, $W_f(E)$ and $W_b(E)$, and the forward and backward reactions paths, to the planes of the normal form coordinates. The volumes enclosed by $W_f(E)$ and $W_b(E)$ project to the darkly shaded regions in the first and third quadrant in the plane of the reaction coordinates, respectively. Their projections to the planes of the bath coordinates coincide with the projection of the NHIM and the dividing surface in Figs. 3 and 4. The forward and backward reaction paths project to hyperbolas (bold curves) in the first and third quadrant in the plane of the reaction coordinates, respectively, and to the origins (bold points) in the planes of the bath coordinates. The lightly shaded regions mark the projections of the energy surface.

reactive volume enclosed by $W_f(E)$ projects to the first quadrant. This projection is bounded by the corresponding hyperbola $q_1 p_1 = \mathcal{I}$, with $\mathcal{I}$ obtained from $H_{\mathrm{NF}}(\mathcal{I},0,...,0) = E$. Likewise, $W_b(E)$ projects to the third quadrant in the (q_1, p_1) plane. $W_f(E)$ encloses *all* forward reactive trajectories; $W_b(E)$ encloses *all* backward reactive trajectories. *All* nonreactive trajectories are contained in the complement of the reactive volumes mentioned above.

The local geometry of $W_f(E)$ and $W_b(E)$ suggests a natural definition of *dynamical* forward and backward reaction paths as the unique paths in phase space obtained by putting all of the energy of a reacting trajectory into the reacting mode, i.e., setting $q_2 = \cdots = q_n = p_2 = \cdots = p_n = 0$. This gives the two hyperbolas $q_1 p_1 = \mathcal{I}$, with $\mathcal{I}$ obtained from $H_{\mathrm{NF}}(\mathcal{I},0,...,0) = E$, which in phase space are contained in the plane of the reaction coordinates, see Fig. 5. This way, the forward (respectively, backward) reaction path can be thought of as the ''center curve'' of the relevant volume enclosed by the forward (respectively, backward) reactive spherical cylinder $W_f(E)$ [respectively, $W_b(E)$]. These reaction paths are the special reactive trajectories which intersect the dividing surface at the ''poles'' (in the sense of North and South poles, where $q_1 = p_1$ assumes its maximum and minimum value on the dividing surface).

5. The transmission time through the transition region

It follows, from the normal form, that trajectories traverse the transition region in a strongly correlated fashion. In order to detect the correlation from the time evolution of neighboring trajectories, one has to take into account the different times scales that it takes for trajectories to traverse the dividing surface region. To see this, we consider trajectories with initial conditions $[q_1(0),...,q_n(0), p_1(0),...,p_n(0)]$, with $p_1 - q_1 = c$ for some constant $c > 0$, i.e., initial conditions which lie on the reactant side of the dividing surface. More precisely, we require that $p_1(0)$ and $q_1(0)$ be positive, so that the resulting trajectory is forward reactive, and ask for the *time of flight* to reach $p_1 - q_1 = -c$ on the product side. The equations of motion yield $q_1(t) = q_1(0)\exp[t(\partial H_{\mathrm{NF}}(\mathcal{I},J_2,...,J_n)/\partial\mathcal{I})]$ and $p_1(t) = p_1(0)\exp[-t(\partial H_{\mathrm{NF}}(\mathcal{I},J_2,...,J_n)/\partial\mathcal{I})]$, where $\partial H_{\mathrm{NF}}(\mathcal{I},J_2,...,J_n)/\partial\mathcal{I}$ is determined by the initial conditions. This gives the time of flight as

$$T = \left(\frac{\partial H_{\mathrm{NF}}(\mathcal{I},J_2,...,J_n)}{\partial\mathcal{I}}\right)^{-1} \ln\left(\frac{p_1(0)}{q_1(0)}\right). \tag{2}$$

The time diverges logarithmically as $q_1(0) \to 0$, i.e., the closer the trajectory starts to the boundary $W_f(E)$. It is not difficult to see that the time of flight is shortest for the center curve of the volume enclosed by $W_f(E)$, i.e., *the trajectory which traverses the transition region fastest is precisely our forward reaction path*. A similar construction applies to backward reactive trajectories.

It should be clear that the normal form allows to scale time for individual trajectories in such a way that they traverse the transition region in a unit time step. In fact, the normal form can be used to map trajectories through the transition region, i.e., the phase space point at which a trajectory enters the transition region can be mapped analytically to the phase space point at which the trajectories exits the transition region.

E. ''Globalizing'' the local transition structures

It is important to understand how the normal form is used to compute local phase space structures since, in general, we do not expect the normal form expansion to converge (see Refs. 36–40, for an overview). The goal is to obtain a neighborhood of the saddle in phase space that is as large as possible, in which the approximation resulting from the truncation of the normal form (to some finite order) yields the ''desired accuracy.'' What we mean by desired accuracy, and how we determine it, will be explained in a moment. This ''neighborhood of validity'' of the normal form in phase space has to be large enough to contain the dividing surface (and hence the NHIM, which is itself contained in the dividing surface) for the energy of interest. The larger the neighborhood of validity, the higher one can go in energy above the energy of the saddle in order to compute the dividing surface, the NHIM, and the local parts of its stable and unstable manifolds. For a given neighborhood of an equilibrium point, we take the normal form computation to successively higher orders until either (i) no improvement in accuracy is seen with increasing order, (ii) the desired accuracy is reached, or (iii) we reach practical limits on the size of our computations. Using the transformations back and forth between the normal form coordinates and the original phase space coordinates, the accuracy of the normal form is determined by a battery of checks, which includes the conservation of the original Hamiltonian on the computed dividing surface (which contains the NHIM), invariance of the computed NHIM under the flow of the *original* Hamiltonian vector field, and conservation of the integrals resulting from the normal form along trajectories computed by integrating the original equations of motion as they pass through the neighborhood under consideration. The normal forms that we use in what follows satisfy all these checks to a very high accuracy, as we will note later.

The NHIM and the dividing surface are compact manifolds, and in this sense local in character. In contrast, the stable and unstable manifolds of the NHIM, and our dynamical reaction paths, are nonlocal in nature. These nonlocal objects, which via the normal form are at first defined only locally in the neighborhood of the saddle, can be ''globalized'' by mapping them, via, the normal form transformation, back into the coordinates of the original Hamiltonian system, and then continuing them numerically out of the neighborhood of validity of the normal form, by integrating the original equations of motion in the appropriate direction in time. It is the high accuracy of the normal form which provides us with high quality initial conditions, so that we can track the stable and unstable manifolds, and the dynamical reaction paths, far away from the neighborhood of validity of the normal form and in this way explore the dynamical roadmap of the energy surface. As we will demonstrate below, the accuracy is so high that we can even study connections homoclinic to, or heteroclinic between, NHIMs.

F. Flux across the dividing surface

In Ref. 8, we prove that our dividing surface minimizes the directional flux. The crucial point is that the Hamiltonian vector field ''pierces'' the forward and backward hemispheres of our dividing surface in different directions, and that the Hamiltonian vector field is tangent to our dividing surface only at the NHIM. A deformation of our dividing surface leads to an increase of directional flux if the points of tangency for the deformation no longer coincide with the NHIM. This increase in flux is due to the fact that such a (generic) deformation is also crossed by nonreactive trajectories (see Ref. 8 for the details). On the other hand, any dividing surface obtained from ours by the special class of deformation, for which the set of points, at which the Hamiltonian vector field is tangent to the deformed dividing surface, still coincides with the NHIM, leads to the same directional flux. In this sense the dividing surface of minimal flux is not unique. In fact, the flux is a quantity which is determined solely by the NHIM. In Ref. 8, we show that, utilizing Stokes' theorem, the flux across the forward and backward dividing surfaces, $B_{ds,f}^{2n-2}(E)$ and $B_{ds,b}^{2n-2}(E)$, can be computed from a generalized action integral over the NHIM. In the case of two DOF, where the NHIM is a periodic orbit, this action integral simply gives the action of the periodic orbit. In particular, the flux is invariant under canonical transformations and can be computed from the normal form. The general result is most elegantly expressed in terms of the actions J_i, $i=2,...,n$, of the bath degrees of freedom. Let $\mathcal{V}(E)$ denote the volume in the $(n-1)$-dimensional space of the positive integrals $J_2,\ldots,J_n$ enclosed by the energy contour $H_{\mathrm{NF}}(0,J_2,\ldots,J_n)=E$, constant. Then the flux through the forward dividing surface $B_{ds,f}^{2n-2}(E)$ is given by

$$N(E)=(2\pi)^{n-1}\mathcal{V}(E). \tag{3}$$

The flux across the backward dividing surface $B_{ds,b}^{2n-2}(E)$ has the same magnitude but opposite sign, so that the total flux across the dividing surface adds up to zero. If we consider only quadratic terms in the Hamiltonian, we obtain the well-known result

$$N(E)=\frac{(2\pi)^{n-1}}{(n-1)!}\frac{E^{n-1}}{\omega_2\cdots\omega_n}. \tag{4}$$

Hence, the normal form expansion allows us to incorporate nonlinear corrections to the flux to any desired order.

The fact, that the flux is a quantity solely determined by the NHIM, is in accordance with the physical significance of the NHIM. As mentioned above, the NHIM is the energy surface of the activated complex, i.e., an invariant subsystem with one degree of freedom less than the full system. In terms of the normal form coordinates, this subsystem is given explicitly by setting the reaction coordinates (q_1,p_1) to zero. Dividing the phase space volume of the activated complex enclosed by the NHIM by the ''elementary'' $(n-1)$ DOF phase space volume, $(2\pi\hbar)^{n-1}$, gives the dimensionless quantity whose quantum statistical interpretation is the mean number of states with energy less than E in the activated complex. In fact, the quantum mechanical interpretation of this quantity is the mean number of open transmission channels and, as well be outlined in the following section, quantum effects can lead to a quantization of the flux.

G. Quantum mechanical effects

Though the main focus of this work is classical mechanics, it is worth mentioning that the geometry of the complexification of the transition structures discussed above offers the opportunity to incorporate quantum effects—at least to the degree of a semiclassical approximation—in a very nice and coherent picture, which we will sketch in the following. There exists a quantum mechanical analog of the Poincaré-Birkhoff normalization procedure, the quantum normal form,[41,42] which in the chemical literature is known as *canonical Van Vleck perturbation theory*.[43] The quantum normal form is complicated by the noncommutativity of the operators which replace the classical phase space coordinates. This can be dealt with by the introduction of an ordering convention. In this way, different orders of the quantum normal form correspond, at the same time, to different orders in Planck's constant.[44] It is well known that the quantum normal form yields excellent results for the computation of quantum spectra of potential wells, i.e., when the normal form is expanded about a center-...-center equilibrium point. However, the quantum normal form similarly applies to equilibria of saddle-center-...-center type, which are relevant in the context of transition state theory. Works in this direction can be found in Refs. 34, 35, 44–46, and in the recent work by Creagh.[47]

For the quantum mechanical system, the actions corresponding to the bath degrees of freedom become quantized, i.e., $J_i(k_i)=\hbar(k_i+1/2)$ with nonnegative integer quantum numbers k_i, $i=2,...,n$. Each mode, defined by a set of quantum numbers $(k_2,\ldots,k_n)$, has its own energy-dependent transmission probability, $P(k_2,\ldots,k_n;E)$, which can be calculated as follows. For a given energy E each mode implicitly fixes the saddle integral $\mathcal{I}$ via the energy equation,

$$H_{\mathrm{NF}}[\mathcal{I}(k_2,\ldots,k_n;E),J_2(k_2),\ldots,J_n(k_n)]=E, \tag{5}$$

where, for simplicity of exposition, we have inserted the quantized bath actions into the classical normal form Hamil-

tonian, and hence ignored the problem of ordering the operators. Up to a prefactor of $-\pi$, the saddle integrals defined this way are identical with the mode-specific *tunnel* or *barrier penetration integrals* (see Ref. 48),

$$\theta(k_2,\ldots,k_n;E) = -\pi \mathcal{I}(k_2,\ldots,k_n;E), \tag{6}$$

which give the transmission probabilities as

$$P(k_2,\ldots,k_n;E) = (1+e^{2\theta(k_2,\ldots,k_n;E)})^{-1}. \tag{7}$$

The tunnel integrals $\theta(k_2,\ldots,k_n;E)$ can be interpreted as the actions of complex tunnelling paths. For a fixed energy, we can associate with each mode $(k_2,\ldots,k_n)$ a toroidal cylinder $T^{n-1}\times\mathbb{R}$, i.e., the product of the $(n-1)$-tori defined by $(p_i^2+q_i^2)=\hbar(k_i+1/2)$, $i=2,...,n$, and the hyperbola defined by $q_1p_1=\mathcal{I}(k_2,\ldots,k_n;E)$. Depending on the mode and on the energy, the trajectories on a toroidal cylinder are nonreacting or reacting depending on whether $\mathcal{I}(k_2,\ldots,k_n;E)$ is negative or positive. Note that the appearance of nonreacting trajectories is not restricted to energies $E<0$; trajectories with $E>0$ can be nonreactive if they have too much energy in the bath modes and, thus, not enough in the reactive mode. For a nonreacting trajectory, the point of closest approach to the saddle is given by the phase space "turning point," where $p_1+q_1=0$ intersects $q_1p_1=\mathcal{I}(k_2,\ldots,k_n;E)$. Depending on whether the toroidal cylinder is on the reactant or the product side of the dividing surface, the turning point is given by $q_{1-}=-p_{1-}=-\sqrt{-\mathcal{I}(k_2,\ldots,k_n;E)}$ or $q_{1+}=-p_{1+}=\sqrt{-\mathcal{I}(k_2,\ldots,k_n;E)}$, respectively. A connection of the turning points by a continuous path on the energy surface can only be accomplished by complexifying the phase space coordinates. More precisely, we keep the bath coordinates real and restrict the complexification to the reaction coordinates (q_1,p_1). For this purpose, it is useful to rotate the reaction coordinates according to

$$\tilde{q}_1=\frac{1}{\sqrt{2}}(q_1-p_1), \quad \tilde{p}_1=\frac{1}{\sqrt{2}}(q_1+p_1), \tag{8}$$

which gives $\mathcal{I}=(\tilde{p}_1^2-\tilde{q}_1^2)/2$. The phase space turning points (q_{1-},p_{1-}) and (q_{1+},p_{1+}) are mapped to $(\tilde{q}_{1-},\tilde{p}_{1-})=[-\sqrt{-2\mathcal{I}(k_2,\ldots,k_n;E)},0]$ and $(\tilde{q}_{1+},\tilde{p}_{1+})=[\sqrt{-2\mathcal{I}(k_2,\ldots,k_n;E)},0]$, respectively. Since the Hamiltonian only depends on the integrals, a connecting path of constant energy requires constant $(\tilde{p}_1^2-\tilde{q}_1^2)/2=\mathcal{I}(k_2,\ldots,k_n;E)$. For the complex tunnelling path, we therefore vary $\tilde{q}_1$ in the real interval $[\tilde{q}_{1-},\tilde{q}_{1+}]$ along which $\tilde{p}_1=(2\mathcal{I}(k_2,\ldots,k_n;E)+\tilde{q}_1^2)^{1/2}$ is purely imaginary. The "action" along this tunneling path is

$$\begin{aligned}\theta(k_2,\ldots,k_n;E) &= i\int_{\tilde{q}_{1-}}^{\tilde{q}_{1+}}\tilde{p}_1 d\tilde{q}_1 \\ &= \int_{\tilde{q}_{1-}}^{\tilde{q}_{1+}}\sqrt{-2\mathcal{I}(k_2,\ldots,k_n;E)-\tilde{q}_1^2}\,d\tilde{q}_1 \\ &= -\pi\mathcal{I}(k_2,\ldots,k_n;E),\end{aligned} \tag{9}$$

which is positive. The projection of the complex tunnelling path to the real normal form coordinate planes is shown in Fig. 6.

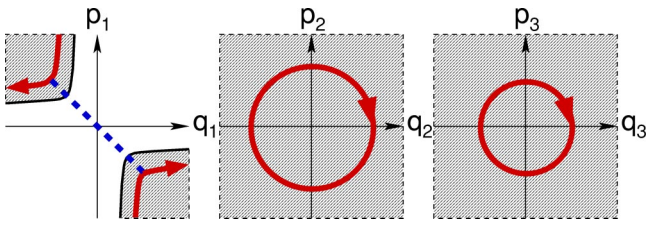

FIG. 6. Projection, to the real planes of the normal form coordinates, of the complex tunneling path (dashed line) connecting nonreactive trajectories (bold curves). The shaded region marks the projections of the energy surface, which has negative energy.

It is important to note that there is also a tunnel integral associated with the toroidal cylinders which have $\mathcal{I}(k_2,\ldots,k_n;E)>0$, i.e., those which carry reacting trajectories. In this case, the turning points become complex: q_{1-} and q_{1+} and likewise p_{1-} and p_{1+} become complex conjugate pairs. In the rotated coordinate system, $\tilde{q}_{1-}$ and $\tilde{q}_{1+}=-\tilde{q}_{1-}$ are purely imaginary and $\tilde{p}_{1-}=\tilde{p}_{1+}=0$. In terms of $(\tilde{q}_1,\tilde{p}_1)$, the tunnel integral is now taken along the complex tunneling path obtained from varying $\tilde{q}_1$ between $\tilde{q}_{1-}$ and $\tilde{q}_{1+}$ along the imaginary axis where $\tilde{p}_1=(2\mathcal{I}+\tilde{q}_1^2)^{1/2}$ is real. This gives the action

$$\begin{aligned}\theta(k_2,\ldots,k_n;E) &= i\int_{\tilde{q}_{1-}}^{\tilde{q}_{1+}}\tilde{p}_1 d\tilde{q}_1 \\ &= i\int_{-i|\tilde{q}_{1-}|}^{i|\tilde{q}_{1+}|}\sqrt{2\mathcal{I}(k_2,\ldots,k_n;E)-\tilde{q}_1^2}\,d\tilde{q}_1 \\ &= -\pi\mathcal{I}(k_2,\ldots,k_n;E),\end{aligned} \tag{10}$$

which, as opposed to Eq. (9), is now negative. The projection of a complex tunneling path connecting reactive trajectories, to the real normal form coordinate planes, is shown in Fig. 7. The tunnel integrals for nonreacting and reacting trajectories together lead to a *uniform* transmission probability, i.e., an expression for the transmission probability which is valid both below and above the barrier.[48]

The quantum mechanical flux $N(E)$ for energy E, the so-called *cumulative reaction probability*, is the sum over the transmission probabilities of all different modes, i.e.,

$$N(E)=\sum_{k_2,\ldots,k_n} P(k_2,\ldots,k_n;E). \tag{11}$$

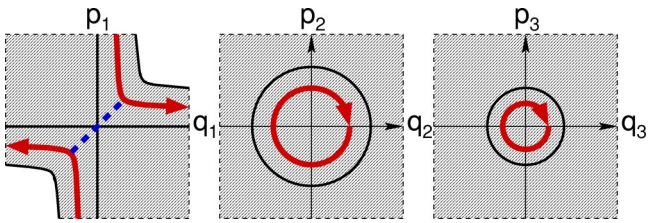

FIG. 7. Projection, to the real planes of the normal form coordinates, of the complex tunneling path (dashed line) connecting reactive trajectories (bold curves). The thin hyperbolas and circles denote the boundaries of the projections of the dividing surface. The shaded region marks the projections of the energy surface, which has positive energy.

This is effectively a summation over switching functions, see Eq. (7). Upon increasing the energy E a mode "opens" as a transmission channel when $P(k_2,\ldots,k_n;E)$ switches from 0 to 1. The energy of the opening of a transmission channel can be defined as the energy for which the tunnel integral $\theta(k_2,\ldots,k_n;E)$ vanishes. The transmission probability $P(k_2,\ldots,k_n;E)$ switches more slowly the stronger the effect of tunneling. Depending on the densities of the energies at which the transmission channels open, and on the intensity of tunneling, the cumulative reaction probability becomes a more or less pronounced step function with plateaus at integer values which give the number of open transmission channels. This "quantization" of the flux has been seen, e.g., in the isomerization of ketene.[49] The analogous effect for ballistic electron transport through narrow constrictions (so-called point contacts), in semiconductor heterostructures and metal nanowires, is the quantization of conductance.[50,51] Without tunneling, the flux as a function of energy increases by 1 each time the contour $H_{\mathrm{NF}}(0,J_2,\ldots,J_n)$ sweeps over a site of the action lattice $J_i=\hbar(n_i+1/2)$, $i=2,\ldots,n$. The complex tunneling path, with its action integral as defined above, gives the tunnelling correction to this flux quantization in a way which takes into account the full *dynamics*.

For the classical system, the "activated complex" defined by $q_1=p_1=0$ gives a true invariant subsystem, with the NHIM being its energy surface. Quantum mechanics tends to wash out the classical phase space structures, abolishing the invariance of the subsystem. Even so, the lifetimes of quantum states of the activated complex can be long enough to become detectable in transition state spectroscopy.[3]

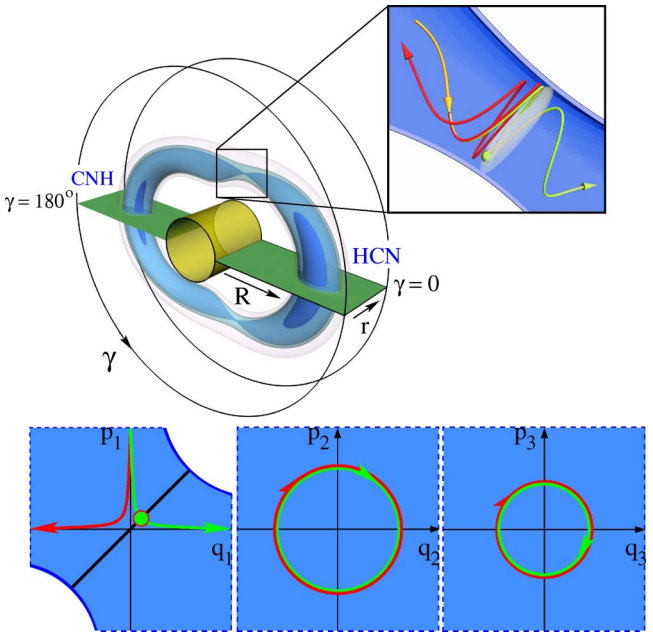

FIG. 8. Jacobi coordinates r, R, and γ, and surfaces of equipotential in 3D, which run from low (dark blue) to high (light blue) energy. The inset shows two initially almost indistinguishable orbits (orange-colored as long as their projections overlap; red and green after they split) with energy 0.2 eV above the saddle. They start on the CNH side of the dividing surface, which is shown as the white translucent object and which has the same energy. The red orbit does not react; the green orbit intersects the dividing surface (at the point marked by the green ball) and hence reacts to the HCN side of the dividing surface. The lower three panels show the same two trajectories as their projections to the planes of the normal form coordinates. The light blue regions mark the projections of the corresponding energy surface. For clarity, the dividing surface (black line segment) and the intersection point of the green trajectory with the dividing surface (bold green dot) are only shown in the projection to the plane of the reaction coordinates (q_1,p_1).

III. ISOMERIZATION OF HCN IN THREE DIMENSIONS

We now apply the theory of Sec. II to a classic problem: the HCN/CNH isomerization reaction. Restricting to vanishing angular momentum, the system has three DOF, the Jacobi coordinates: r (distance between C and N), R (distance between H and the center of mass of C and N) and γ (angle between H and C as seen from the center of mass of C and N). The corresponding Hamiltonian is

$$H=\frac{1}{2\mu}p_r^2+\frac{1}{2m}p_R^2+\frac{1}{2}\left(\frac{1}{\mu r^2}+\frac{1}{mR^2}\right)p_\gamma^2+V(r,R,\gamma), \tag{12}$$

where $\mu=m_{\mathrm{C}}m_{\mathrm{N}}/(m_{\mathrm{C}}+m_{\mathrm{N}})$ is the reduced mass of the CN diatom, $m=m_{\mathrm{H}}(m_{\mathrm{C}}+m_{\mathrm{N}})/(m_{\mathrm{H}}+m_{\mathrm{C}}+m_{\mathrm{N}})$ is the reduced mass of the full system, and the potential V is taken from Murrell and co-workers.[52] There are two saddle-center-center equilibria which are relevant for the isomerization. They are related by reflection symmetry and have $\gamma=\pm\gamma^*\approx\pm 67°$, see Fig. 8.

To these equilibria, we apply the normal form procedure individually which, for a neighborhood of each equilibrium, yields explicit maps between the original Jacobi coordinates and conjugate momenta, $(r,R,\gamma,p_r,p_R,p_\gamma)$, and the new normal form coordinates, $(q_1,q_2,q_3,p_1,p_2,p_3)$. The normal form expansion is carried out to tenth order, i.e., the normal form Hamiltonian may be written as a sum of homogeneous polynomials of degree up to 10 in the normal form coordinates. Most of our calculations are for an energy 0.2 eV above the saddle energy. On the corresponding energy surface, we define "neighborhoods of validity" by delimiting the Jacobi angle according to $|\gamma\pm\gamma^*|<6°$. The accuracy of the normal form in the neighborhoods defined in this way is excellent. As trajectories [integrated with respect to the original equations of motion resulting from Hamilton's equations with the Hamiltonian (12)] pass through these neighborhoods, the integrals $\mathcal{I}$, J_2, and J_3, of the normal form, are conserved to at least ten decimal places.

The inset in Fig. 8 shows the 4D (in phase space) dividing surface calculated from the normal form for an energy 0.2 eV above the energy of the saddle as its projection to configuration space. It completely fills the "bottleneck" in the isopotential surface in configuration space. In fact, the dividing surface fills the bottleneck not only in this projection to configuration space but, more importantly, in the full 5D energy surface.

The inset in Fig. 8, moreover, shows the different fates of two orbits, that are initially very close together, as they approach the dividing surface. The initial conditions of the orbits are so close together that they are indistinguishable on the scale of this picture. In the inset, the two orbits therefore appear as a single orange-colored trajectory on the CNH side of the dividing surface, which splits into a green and a red

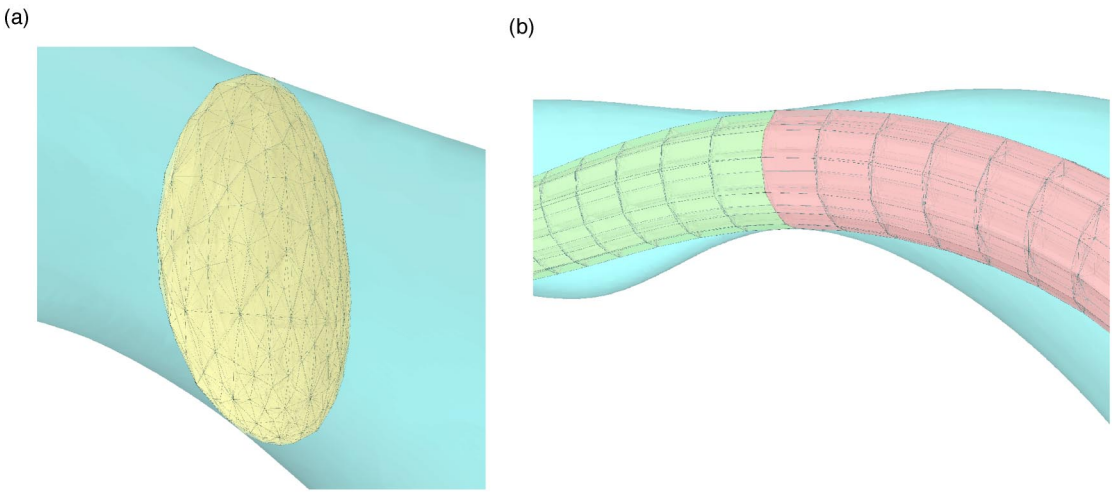

FIG. 9. (a) The configuration space projection of the NHIM (yellow) for a similar inset as in Fig. 8. The turquoise translucent object is the surface of equipotential. (b) The configuration space projection of the forward and backward branches of the stable and unstable manifolds of the NHIM in (a). The green object is the forward branch of the stable manifold, $W_f^s(E)$; the red object is the forward branch of the unstable cylinder, $W_f^u(E)$. In the projection to configuration space, the forward and backward branches of the stable manifold $W_f^s(E)$ and $W_b^s(E)$ coincide with the corresponding branches of the unstable manifold $W_f^u(E)$ and $W_b^u(E)$. In both figures, the energy is 0.2 eV above the energy of the saddle.

trajectory in the diagram as the two constituent trajectories move apart from each other. Once they reach the dividing surface, the green trajectory makes a single passage through the dividing surface in phase space, i.e., it reacts. The configuration space projection of its intersection point with the 4D (in phase space) dividing surface is marked by the green ball. The red trajectory, despite its close approach to the dividing surface, instead ''veers off'' at the last moment, i.e., it does not react.

The explanation for the different behaviors of the trajectories becomes apparent when we analyze them in terms of the normal form coordinates. The trajectories are obtained by integrating the original equations of motion, i.e., Hamilton's equations derived from the Hamiltonian in Jacobi coordinates (12). As the trajectories pass through the neighborhood of validity of the normal form, we apply the normal form transformation from the Jacobi coordinates $(r,R,\gamma,p_r,p_R,p_\gamma)$ to the normal form coordinates $(q_1,q_2,q_3,p_1,p_2,p_3)$. In the lower three panels in Fig. 8, we show the resulting projections of the trajectories to the planes of the normal form coordinates. In the plane of the reaction coordinates (q_1,p_1), we also show the projection of the dividing surface. It locally divides the energy surface into two components: the component which has $p_1-q_1>0$ corresponds to the CNH isomer; the component which has $p_1-q_1<0$ corresponds to the HCN isomer. Both trajectories start on the side of the CNH isomer. In the plane of reaction coordinates, the green and the red trajectory project to hyperbolas in the first and second quadrant, respectively. The green trajectory is thus contained in the reactive energy surface volume enclosed by the forward reactive spherical cylinder, while the red trajectory is not. The green ball indicates once again the point of passage through the dividing surface.

Because of the simplicity of the equations in the normal form coordinates, we can ''tailor'' reacting and nonreacting trajectories of virtually any possible allowable type by the globalization procedure we explained in Sec. II E. We therefore choose initial conditions in the normal form coordinates, map them back to the Jacobi coordinates and then integrate Hamilton's equations of motion derived from the Hamiltonian (12).

In Fig. 9, we show the configuration space projection of cell-complexes (meshes) in phase space, computed on the NHIM and its stable and unstable manifolds. While the NHIM is, like the dividing surface in Fig. 8, computed completely from the normal form, its stable and unstable manifolds are obtained by globalizing their local parts obtained from the normal form, as described above. The NHIM, which is 3D in phase space, projects to a 3D object in configuration space. Likewise, its stable and unstable manifolds, which are 4D in phase space, map to 3D objects in configuration space. The property of the Hamiltonian (12) of being quadratic in the momenta implies a time-reversal symmetry, which causes the configuration space projections of the stable and unstable cylinders to coincide. This would not be the case if the Hamiltonian function contained rotational or magnetic terms. We emphasise again that the approach that we present here can also handle such terms without difficulty.[53]

It is important to note that, under generic conditions for three DOF systems, the projection to configuration space of the NHIM will be a ''solid'' three-dimensional object, as exemplified by the HCN isomerization system that we study here. If we impose the restrictions of no local recrossing and minimization of the flux, it may be shown that[8] the NHIM must ''separate'' the halves of the dividing surface that correspond to forward and backward trajectories. These geometrical considerations are a further indication of the *impossibility* of defining a dividing surface, which has the bottleneck property explained in Sec. II B and which minimizes the flux, as a surface in configuration space. We emphasize here that the definition of these objects that we give in phase space has exactly the required properties.

A. The reaction path

As we mentioned in Sec. II D 4, our dynamical reaction paths are defined by setting the bath coordinates (q_2,q_3,p_2,p_3) equal to zero, i.e., ''no energy in the bath modes.'' As a consequence, the reaction paths are contained in the plane of the reaction coordinates (q_1,p_1). In Fig. 8, they coincide with the boundary curves of the projection of the energy surface to the plane of the reaction coordinates (q_1,p_1). The forward reaction path from CNH to HCN is in the first quadrant; the backward reaction path from HCN to CNH is in the third quadrant. These curves are mapped back into the original Jacobi coordinates via the normal form transformation and then globalized by integrating them outside the neighborhood where the normal form is valid. In Fig. 10, we show the configuration space projections of reaction paths computed in this way for a range of energies. Although the forward and backward reaction paths are different curves in phase space, their projections to configuration space coincide because of the time-reversal symmetry for this particular system. As mentioned above, this would not be the case if the Hamiltonian function contained rotational or magnetic terms.

For comparison, Fig. 10 also shows the minimum energy path, i.e., the path which joins the potential saddle with the HCN and CNH potential minima along a curve in configuration space which is perpendicular to the equipotentials. The minimum energy path is of importance for the study of the topographical aspects of potential energy surfaces such as, e.g., the global connectivity of local potential minima (see, e.g., Ref. 22). The dynamical significance of minimum energy paths is restricted to systems which are coupled to a heat bath. The coupling is typically incorporated by introducing friction and thermal noise into the system. In this case, the deterministic ''dynamics'' of the system (obtained from neglecting the thermal noise) follows the minimum energy path in the limit of high friction (which slows the system down and essentially removes all dynamical effect). The minimum energy path is, moreover, the starting point for many statistical approaches to reaction rate calculations for systems coupled to a heat bath. The main idea is to compute a mean force from differences in free energy along the minimum energy path. The free energy at a given point on the minimum energy path is obtained from a constrained configuration space average over the hyperplane which intersects the minimum energy path at that point ''perpendicularly.'' The assumption of ergodicity of the motion always underlies such approaches. This assumption is brought into question (at least in the small friction limit) since we have seen, in Sec. II C, that the motion of a system without heat bath is integrable in a neighborhood of the saddle.

Figure 10 shows that our reaction paths, which incorporate the full effect of the dynamics, do not follow the minimum energy path. As mentioned in Sec. II D 4, the forward and backward reaction paths are the center curves of the reactive volumes enclosed by the forward and backward reactive spherical cylinders, respectively. They map to the origins of the planes of the bath coordinates (q_2,p_2) and (q_3,p_3). A typical reactive trajectory also has energy in the bath modes and describes circular motions in the bath DOF.

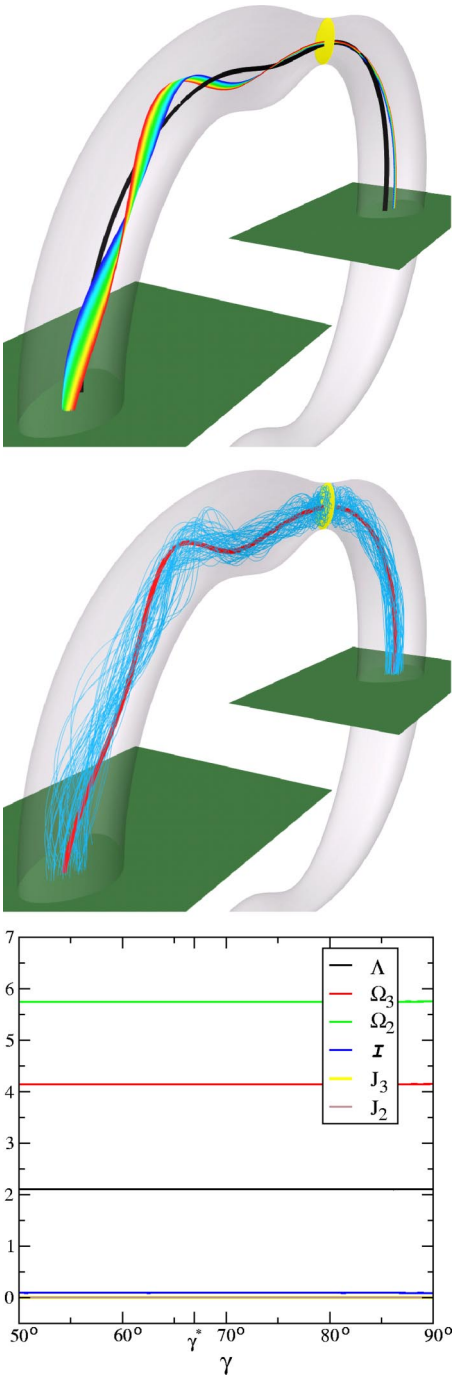

FIG. 10. The top panel shows the minimum energy path in black. The rainbow colored belt shows our reaction paths corresponding to energies ranging from the energy of the saddle (blue) to 0.2 eV above the saddle (red). The translucent object is the surface of equipotential for 0.2 eV above the saddle. The middle panel shows a bundle of trajectories (blue) for energy $E=0.2$ eV above the saddle energy. The trajectories are contained in the energy surface volume enclosed by the forward reactive spherical cylinder $W_f(E)$. They spiral about our forward reaction path (red), which is the ''center curve'' of this volume in phase space. The dividing surface is shown in yellow. The bottom panel shows the values of the integrals $\mathcal{I}$, J_2, and J_3, and nonlinear frequencies $\Lambda\equiv\partial H_{\mathrm{NF}}((\mathcal{I},J_2,J_3)/\partial\mathcal{I}$, $\Omega_2\equiv\partial H_{\mathrm{NF}}((\mathcal{I},J_2,J_3)/\partial J_2$ and $\Omega_3\equiv\partial H_{\mathrm{NF}}((\mathcal{I},J_2,J_3)/\partial J_3$, along a segment of our reaction path in the middle panel (shown in terms of its Jacobi angle γ).

This leads to a spiraling of the reactive trajectory about the reaction path. This is illustrated in the middle panel in Fig. 10 which shows the configuration space projection of a bundle of forward reactive trajectories in a single energy

surface spiralling about the corresponding forward reaction path.

In the bottom panel of Fig. 10 we show the values of $\mathcal{I}$, J_2, and J_3, and the values of the nonlinear frequencies ($\partial H_{\mathrm{NF}}/\partial \mathcal{I}$, $\partial H_{\mathrm{NF}}/\partial J_2$, and $\partial H_{\mathrm{NF}}/\partial J_3$), along a long segment of our forward reaction path for an energy 0.2 eV above the saddle energy. Although the Jacobi angle γ of this segment varies between 50° and 90°, i.e., the segment extends far beyond the neighborhood of validity of the normal form, which we defined by delimiting the Jacobi angle according to $|\gamma \pm \gamma^*| < 6°$, both the integrals and the nonlinear frequencies are constant on the scale of the figure. This emphasizes in an impressive way the high quality of the normal form approximation. Recall that, within the neighborhoods of validity of the normal form, these quantities are conserved to at least ten decimal places.

B. Following reacting trajectories into the potential wells

All reactive trajectories on an energy surface of energy above the saddle are contained in the relevant volumes enclosed by the forward and backward reactive spherical cylinders, $W_f(E)$ and $W_b(E)$. The ability to "globalize" $W_f(E)$ and $W_b(E)$, and hence to track them far away from the regions of validity of the normal form, gives us the opportunity to find initial conditions of reacting trajectories far away from the transition regions. Moreover, this gives us the opportunity to study how reacting trajectories become temporarily trapped in the potential wells.

To demonstrate this, we consider a surface of section (SOS) in the "bottom" of the HCN well, which we define by $\gamma=0$, $p_\gamma \leqslant 0$. In fact, on a fixed energy surface, the section condition $\gamma=0$ defines a four-dimensional sphere which can be considered to consist of the two hemispheres which have $p_\gamma > 0$ and $p_\gamma < 0$, respectively. The "equator" of this four sphere, which coincides with the boundary of the SOS, has $p_\gamma = 0$. This is nice because $\gamma = p_\gamma = 0$ defines an invariant system, i.e., a trajectory starting with $\gamma = p_\gamma = 0$ will retain $\gamma = p_\gamma = 0$ for all time. It is easy to see that $\dot{\gamma} < 0$ everywhere on the SOS except for the boundary. Hence, the SOS is a good choice as it is transverse to the Hamiltonian flow except for the boundary, which is invariant. This SOS allows us to study how trajectories, which move from the CNH region into the HCN region through the dividing surface at $+\gamma^*$, evolve through the HCN well and possibly reach the dividing surface at $-\gamma^*$ or return back to the dividing surface at $+\gamma^*$.

The complete 4D SOS is hard to visualize. Instead, we visualize part of it by choosing points (r,R) with $\gamma=0$ in configuration space. For fixed (r,R,γ), the energy equation

$$\frac{1}{2\mu}p_r^2 + \frac{1}{2m}p_R^2 + \frac{1}{2}\left(\frac{1}{\mu r^2} + \frac{1}{mR^2}\right)p_\gamma^2 = E - V(r,R,\gamma), \tag{13}$$

defines a two-dimensional sphere in (p_r, p_R, p_γ). The restriction to $p_\gamma \leqslant 0$ selects one hemisphere, a two-dimensional disk, from this two sphere. Note that the boundary of this disk has $p_\gamma = 0$ and is hence contained in the boundary of the four-dimensional SOS. As coordinates on the two-dimensional disk, we choose the momenta p_r and p_R. Figure 11 shows this construction for two different configuration space points (r,R) (with $\gamma=0$). The top panel in Fig. 11 corresponds to the HCN potential minimum, which has $(r,R) \approx (1.153\,216, 1.686\,416\ \text{Å})$. The differently colored regions correspond to different types of trajectories. Points in the blue and light green regions correspond to initial conditions which, when integrated backward in time, directly (i.e., without a further intersection with the SOS) reach the dividing surface at $+\gamma^*$. The blue and light green regions thus correspond to the reactive energy surface volume enclosed by the respective unstable spherical cylinder branch of the NHIM at $+\gamma^*$. Initial conditions in the red and light green regions correspond to trajectories which, when integrated forward in time, directly reach the dividing surface at $-\gamma^*$, i.e., the red and light green regions correspond to the reactive energy surface volume enclosed by the respective stable spherical cylinder branch of the NHIM at $-\gamma^*$. The light green region is the overlap region between the two volumes. Initial conditions in the light green region correspond to trajectories which entered the HCN well through the dividing surface at $+\gamma^*$ and, with only one intersection with the SOS, exit the HCN well through the dividing surface at $-\gamma^*$.

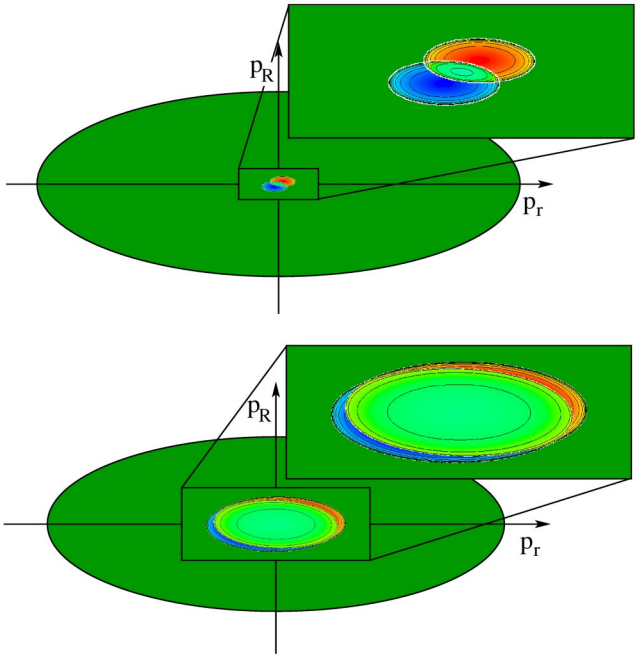

FIG. 11. Pieces of the 4D SOS in the HCN potential well. The top panels corresponds to the HCN potential minimum; the bottom panel corresponds to the intersection of our reaction path, see text. The eccentricities of the individual ellipses and the relative sizes of the ellipses are authentic in the main left-hand panels (in the right-hand insets, which show magnified images of the left-hand panels, different scale factors have been used in order to show the structures more clearly).

The boundary of the blue patch consists of the first intersection of the unstable manifold of the NHIM at $+\gamma^*$ with the SOS (the bottom arc which is the border to the dark green region) and the first intersection of the stable manifold of the NHIM at $-\gamma^*$ with the SOS (the top arc which is the border to the light green region). Here "first intersection" refers to the intersection of the unstable/stable manifolds

with the SOS which occurs first when they are followed from the NHIM. Similarly, the boundary of the red patch consists of the first intersection of the stable manifold of the NHIM at $+\gamma^*$ with the SOS (the top arc which is the border to the dark green region) and the first intersection of the unstable manifold of the NHIM at $+\gamma^*$ with the SOS (the bottom arc which is the border to the light green region).

The contours in the blue region are curves of equal time it takes the trajectories intersecting in this region to evolve from the dividing surface at $+\gamma^*$ to the SOS. Similarly, the contours in the red region show the times it takes the initial conditions to reach the dividing surface at $-\gamma^*$. The contours in the light green region show the times the trajectories spend in the HCN well after entering the HCN well through the dividing surface at γ^* and before leaving the HCN well through the dividing surface at $-\gamma^*$.

In accordance with the calculation in Sec. II D 5, the times in the blue region diverge logarithmically upon approaching the bottom boundary arc, and the times in the red region diverge logarithmically when they approach the top boundary arc. In the light green region, the time diverges upon approaching either boundary arc.

The small size of the patches indicates that only a tiny fraction of trajectories starting on the dividing surface near $-\gamma^*$ pass near the HCN equilibrium in configuration space. In fact, if we choose $(r,R)\approx(1.179\,069,1.798\,676\,\text{Å})$, which are the configuration space variables which correspond to the intersection of our forward reaction path emanating from the dividing surface at $+\gamma^*$ with the SOS, the patches are *much* larger, see the bottom panel in Fig. 11. This shows that most trajectories ''avoid'' the HCN potential minimum and the minimum energy path, and that our dynamical reaction path is much better suited to characterizing which initial conditions in the well will react.

The first intersection of the unstable spherical cylinder branch of the NHIM at γ^* with the SOS is a 3-sphere. It encloses a four-dimensional ball in the SOS. The blue and light green regions in Fig. 11 are part of this ball. Likewise, the first intersection of the stable cylinder branch of the NHIM at $-\gamma^*$ with the SOS is also a 3-sphere which encloses a four-dimensional ball in the SOS. The red and light green regions in Fig. 11 correspond to this ball. The conservation of flux along the stable and unstable spherical cylinders implies that the flux through these balls is equal to the directed flux through the dividing surface at $+\gamma^*$ or, equivalently, at $-\gamma^*$.[22] Since the overlap between these balls is not complete, trajectories which react from CNH to HCN can become temporarily trapped in the HCN well. Note that, for reasons of flux conservation, such trajectories cannot become permanently trapped in the HCN well (permanent trapping is possible only for a set of trajectories which is of measure zero). Understanding how trajectories get temporarily trapped is the key to rate calculations.

Statistical rate theories typically assume that reactive trajectories explore the potential wells ergodically. According to the microcanonical version of Rice-Ramsperger-Kassel-Marcus (RRKM) theory (see, e.g., Ref. 54 and the references therein), the rate for escape from the HCN well (treating the CNH well as an infinite sink from which trajectories cannot return) would be given by

$$\kappa = 2\frac{N(E)}{Z(E)}, \tag{14}$$

where $N(E)$ is the positive flux through one of the dividing surfaces (e.g., the one near $+\gamma^*$) and $Z(E)$ is the volume of the energy surface component associated with the HCN isomer. The factor 2, in the above equation, incorporates the fact that there are two dividing surfaces through which trajectories can escape. The idea of expressing rates as the flux over energy surface volumes has been taken up by De Leon and co-workers[55,56] in order to refine RRKM theory by applying it to smaller divisions of the energy surface to obtain more details about the dynamics. This leads to so-called reactive island (RI) theory. The main problem in RRKM theory, which persists in the form of RI theory used by De Leon and co-workers, is the assumption that the reactive trajectories explore the potential wells ergodically. This is not true for HCN/CNH isomerization. In fact, only a fraction of initial conditions in the HCN well lead to reactive trajectories. In a forthcoming paper[57] we will provide a procedure to determine this reactive energy surface volume which mainly exploits the theory presented in this paper.

C. Homoclinic and heteroclinic connections: The skeleton of rare events

A typical feature of complex systems like, e.g., clusters, glasses, or proteins, is the coexistence of several dividing surfaces (see, e.g., Ref. 22 and the references therein). A basic example is a potential energy surface with two deep potential minima (corresponding, e.g., to two ''stable'' isomers of a cluster) and a landscape with several local minima and saddles inbetween. In order to react, trajectories have to find their way through one or more, possibly competing, successions of dividing surfaces. A significant problem in determining and sampling such important trajectories numerically, in molecular dynamics simulations, is the presence of very different time scales: transitions are infrequent, or ''rare,'' events on the time scale that a trajectory spends in a deep potential well.

Most developments of statistical sampling techniques for rare events focus on thermal systems which have friction and stochastic forces due to coupling to a heat bath.[20,58] These techniques typically encounter numerical problems in the Hamiltonian limit of vanishing friction. For Hamiltonian systems, on the other hand, there exists a strongly geometrically oriented theory of phase space transport which does not make assumptions of ergodicity (see Refs. 4 and 5) and this allows for the investigation of nonstatistical effects like non-Markovian behavior or *dynamical memory*. Our present work provides some first steps to implementing these ideas for systems with many degrees of freedom.

A reactive trajectory approaches a dividing surface within the relevant energy surface volume enclosed by the respective stable spherical cylinder branch of the corresponding NHIM, and leaves it within the corresponding energy surface volume enclosed by the respective unstable spherical

cylinder branch. A homoclinic orbit to an invariant manifold is an orbit that is in both the stable and the unstable manifold of that invariant manifold (where the invariant manifold could be either the NHIM, a torus in the NHIM, or a periodic orbit in the NHIM). A heteroclinic orbit between two invariant manifolds is an orbit that is in the stable manifold of one invariant manifold and the unstable manifold of the other invariant manifold. Hence, a single heteroclinic orbit is not, in itself, a mechanism for recurrent trajectories, i.e., trajectories that leave and return to the same neighborhood in phase space. However, a heteroclinic *cycle* provides just such a mechanism. A heteroclinic cycle is the union of two, or more, heteroclinic orbits. Since two is the relevant number for HCN isomerization, we will restrict our description to this case. Here, a heteroclinic cycle is the union of a heteroclinic orbit going from NHIM 1 to NHIM 2 (in the sense of direction of motion of the trajectory) and a heteroclinic orbit going from NHIM 2 to NHIM 1. It provides a mechanism for trajectories ''near'' the heteroclinic cycle to leave a neighborhood of either NHIM 1 or 2, and return to that same neighborhood at some later time. For this reason questions of *global* recrossing of dividing surfaces are inherently connected to the existence of *homoclinic* intersections between the stable and unstable manifolds of the same NHIM and *heteroclinic* cycles formed from intersections of the stable and unstable manifolds of different NHIMs.

Recently, we have developed an efficient procedure for computing these intersections[53] corresponding to homoclinic and heteroclinic orbits. The procedure makes use of the Hopf fibration of the NHIM, see Sec. II D 3. The 2-tori of the Hopf fibration are partially hyperbolic and have three-dimensional stable and unstable manifolds, which in normal form coordinates are again described by explicit formulas, namely the stable manifold has $q_1=0$ and the unstable manifold has $p_1=0$. Hence, just as the 2-tori are contained in the NHIM, so their stable and unstable manifolds are contained in the stable and unstable manifolds of the NHIM. For a fixed 2-torus in the NHIM near the saddle at $+\gamma^*$, we consider initial conditions which we displace slightly along the unstable manifold branch which is directed towards the HCN well. When integrated backwards in time these initial conditions will approach the 2-torus asymptotically. We integrate these initial conditions forward in time with respect to the original equations of motion in terms of the Jacobi coordinates, so that they can leave the neighborhood of validity of the normal form and enter the region of the HCN well. Each time the trajectory enters the validity neighborhoods of the normal forms near the saddles at $+\gamma^*$ and $-\gamma^*$, we check whether the trajectory crosses the respective dividing surface contained in that neighborhood, i.e., whether the trajectory is about to react from HCN to CNH across the dividing surface near $\gamma=+\gamma^*$ or the dividing surface near $\gamma=-\gamma^*$. If this is the case, we stop the integration of the trajectory and record the value of the saddle integral $\mathcal{I}$. This way we obtain a map from initial conditions to values of the saddle integral, which we denote $\mathcal{I}_{+\gamma^*}$ or $\mathcal{I}_{-\gamma^*}$ depending on whether the crossed dividing surface is at $+\gamma^*$ or $-\gamma^*$. Recall that $\mathcal{I}=q_1p_1$, and that $q_1=0$ and $p_1=0$ are the stable and unstable manifolds of the NHIM. Hence, $\mathcal{I}_{+\gamma^*}=0$ corresponds to a homoclinic connection to the NHIM which contains the 2-torus near which we started the integration of the trajectory, and $\mathcal{I}_{-\gamma^*}=0$ corresponds to a heteroclinic connection between the different NHIMs near $+\gamma^*$ and $-\gamma^*$.

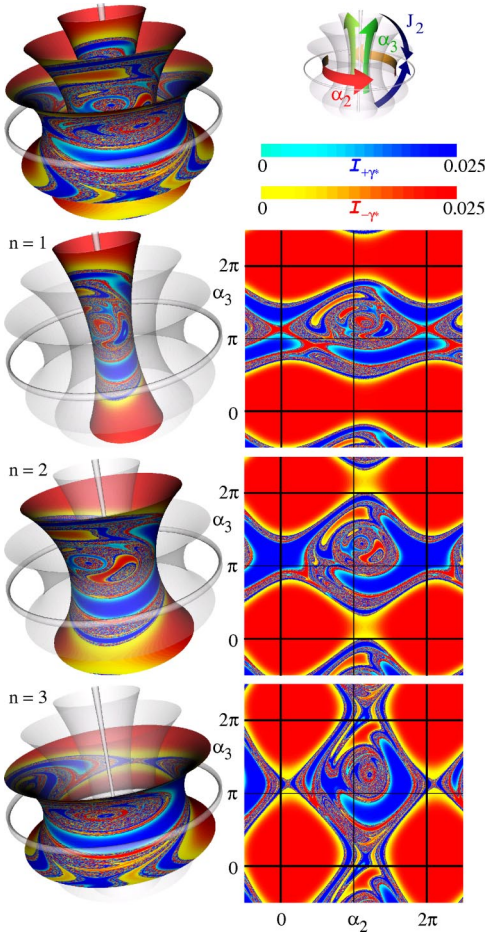

FIG. 12. The left-hand column highlights, schematically, individual 2-tori in the Hopf fibration of the NHIM near $+\gamma^*$ that (when displaced along one branch of the corresponding unstable manifold) generate initial conditions for our computational method. Also shown, on these 2-tori, are contours of values of the integrals $\mathcal{I}_{+\gamma^*}$ and $\mathcal{I}_{-\gamma^*}$, obtained after the initial conditions are integrated into a neighborhood of the saddles at $+\gamma^*$ or $-\gamma^*$, respectively, at the point where they first cross a dividing surface. The 2-tori are for $J_2=nJ_{2\,\max}/4$, $n=1, 2, 3$, where $J_{2\,\max}$ is the maximum J_2 on the NHIM. The values $n=0$ and $n=4$ correspond to the two Lyapunov periodic orbits which have $J_2=0$ or $J_3=0$, respectively. The 2-tori are parametrized by the angles α_2 and α_3 conjugate to J_2 and J_3. For clarity, the right hand panels show the 2-tori in the covering space. The energy is 0.2 eV above the saddle.

In Fig. 12, we show the Hopf fibration of the NHIM near $+\gamma^*$ schematically, together with contours of the map just described. Homoclinic orbits to the same NHIM correspond to zeros $\mathcal{I}_{+\gamma^*}=0$, i.e., to the boundaries of the blue patches. Heteroclinic orbits between different NHIMs correspond to zeros $\mathcal{I}_{-\gamma^*}=0$, i.e., to the boundaries of the red/yellow patches. Though the individual regions in Fig. 12 themselves are regular, in the sense that they each have a smooth boundary, the disposition of the regions is very intricate. We illustrate this by repeating the procedure described above for initial conditions on the two-dimensional unstable manifold of the Lyapunov orbit near the saddle at $+\gamma^*$ which has $J_2=0$. Integrating these initial conditions forward in time, if they return to a neighborhood of the saddle at $+\gamma^*$ or the

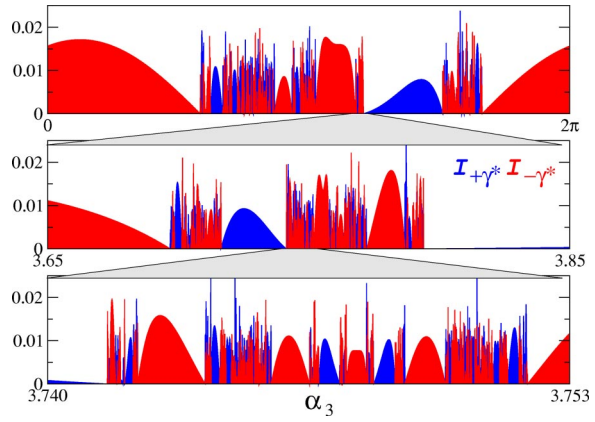

FIG. 13. Graphs of $\mathcal{I}_{+\gamma^*}$ and $\mathcal{I}_{-\gamma^*}$ as functions of the angle conjugate to J_3. The zeros correspond to orbits homoclinic to, and heteroclinic between, the Lyapunov orbit near the saddle at $+\gamma^*$ and the NHIMs near the saddles at $+\gamma^*$ and $-\gamma^*$. The three panels show successive magnifications of smaller regions, from which we see a self-similar structure.

saddle at $-\gamma^*$, where the normal forms are valid, we plot the value of $\mathcal{I}_{+\gamma^*}$ (in blue) or $\mathcal{I}_{-\gamma^*}$ (in red) as a function of the angle conjugate to J_3 along the Lyapunov orbit. These are shown in the top panel of Fig. 13. Since these functions are highly oscillatory, for visualization purposes we also color the region under the value of the function with the corresponding color. Each zero of $\mathcal{I}_{+\gamma^*}$ in blue or $\mathcal{I}_{-\gamma^*}$ in red indicates the existence of an initial condition which in time is backward asymptotic to the Lyapunov orbit and forward asymptotic either to the NHIM near $+\gamma^*$ (blue) or to the NHIM near $-\gamma^*$ (red), respectively. The two panels below the top panel in Fig. 13 represent successive magnifications of smaller regions of the top panel. From these, one sees a self-similar structure well known from classical scattering systems.[59]

Due to the foliation of the NHIM in terms of invariant 2-tori and two Lyapunov periodic orbits, an orbit which in time is asymptotic to the NHIM is automatically asymptotic to exactly one of its tori or its periodic orbits. The method described above therefore allows us to calculate all kinds of homoclinic and heteroclinic connections. We can refine the locations of suitable initial conditions to extremely high accuracy by employing a shooting method between the $\mathcal{I}$ fibers of the locally valid normal forms. Figure 14 shows some examples. We note that all trajectories shown are integrated numerically from the original equations of motion in terms of Jacobi coordinates. The normal form yields the geometric structures and provides us with the relevant initial conditions.

D. A mechanism for chaos: A new type of "chaotic saddle"

If, besides incorporating the saddle integral $\mathcal{I}$ we also include the bath mode integrals, J_2 and J_3, we are able to calculate orbits which are homoclinic to a *single* 2-torus in a NHIM. Homoclinic connections provide the main mechanism for chaos in Hamiltonian systems. It is proven that homoclinic connections associated with hyperbolic periodic orbits or special types of equilibrium points lead to a *chaotic*

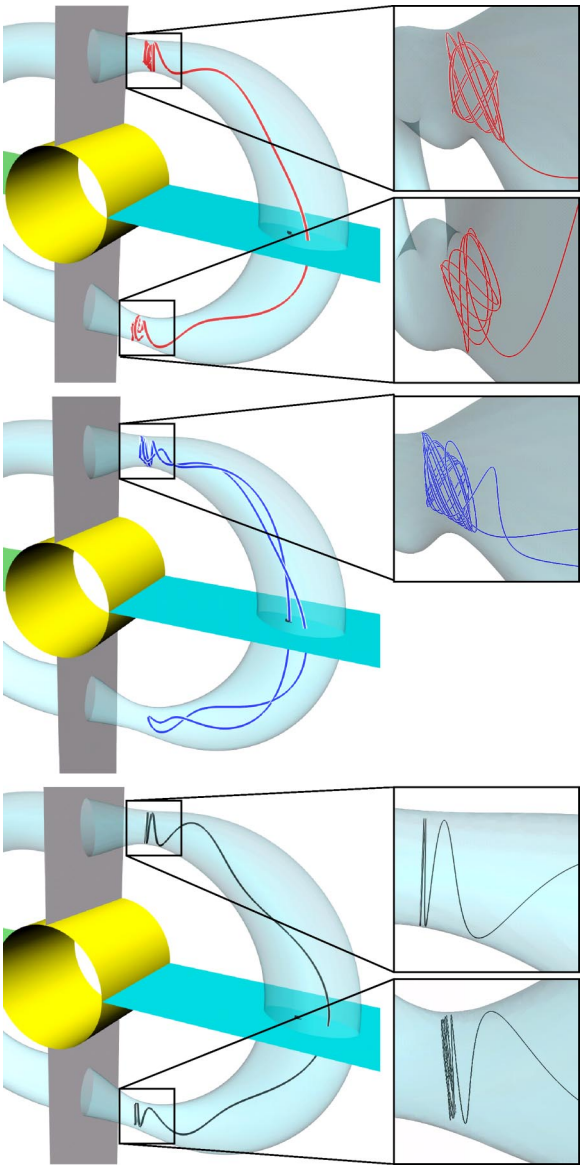

FIG. 14. The top panel shows a heteroclinic connection between a 2-torus in the NHIM near the saddle at $+\gamma^*$ and a 2-torus in the NHIM at $-\gamma^*$. The middle panel shows a homoclinic connection to a *single* 2-torus in the NHIM at $+\gamma^*$. The lower panel shows a heteroclinic connection between a Lyapunov periodic orbit in the NHIM at $+\gamma^*$ and a 2-torus in the NHIM at $-\gamma^*$. The energy in all pictures is 0.2 eV above the saddle energy.

saddle, i.e., to a (uniformly) hyperbolic invariant Cantor set on which the dynamics is conjugate to a shift map. Chaotic saddles play a central role in many complex dynamical phenomena, e.g., the existence of supertransients[60] and the fractal structure of chaotic scattering.[61] There is, as yet, no mathematical proof for chaotic saddles due to homoclinic connections of a normally hyperbolic invariant sphere. Recently progress was made concerning this problem by Cresson[62] who proved the existence of a chaotic saddle for each of the invariant 2-tori foliating the NHIM which have a homoclinic connection. Our procedure described in Ref. 53 allows one to compute these homoclinic connections and hence to detect chaotic saddles. The middle panel of Fig. 14 shows an example of a homoclinic connection to a single 2-torus in the NHIM near the saddle at $+\gamma^*$. Continuation

arguments show that such homoclinic connections exist to every 2-torus in the NHIM. In fact, when the effect of the neglected terms in the normal form expansion (i.e., the nonnormalized ''tail'' of the expansion) are included, we expect, by KAM theory, that a Cantor set of nonresonant tori in the Hopf fibration will persist. This implies the existence of a complicated Cantor set of chaotic saddles which, in turn, implies a complicated ''large'' set of periodically recurrent orbits of arbitrary length. This may provide a dynamical mechanism for so-called entropic barriers (see, e.g., Ref. 63).

IV. CONCLUSIONS AND OUTLOOK

In this paper, we have described a theory for reaction dynamics in phase space, and demonstrated its application to HCN isomerization in three dimensions. The methods developed in this paper offer the opportunity to study fundamental questions concerning both local and global aspects of reaction dynamics in multidimensional systems. The theory is applicable in a broad variety of systems that possess reaction-type dynamics, namely, those associated with saddle-center-...-center equilibrium points. It enables the construction of a *global dynamical roadmap* for energy surfaces which are (energetically) close to these ''saddles.''

The theory, which has no principle limitations concerning the number of degrees of freedom, provides an algorithm for constructing a phase space dividing surface. This dividing surface has the bottleneck property; it divides the energy surface locally into two components (reactants and products) and the only way in which a trajectory can pass from one component to the other is to pass through the dividing surface. Moreover, it is free of local recrossings (reactive trajectories cross it exactly once in the local region, and nonreacting trajectories do not cross it at all) and minimizes the flux. The basic building block of our theory is a normally hyperbolic invariant manifold (NHIM) which controls both the geometry and the dynamics on the energy surface. The existence of the NHIM puts on a rigorous mathematical foundation the concept of an *activated complex* or invariant ''supermolecule,'' located between reactants and products, that has been observed in experiments. The theory also enables us to construct the phase space conduits that trajectories must follow in order to react; the stable and unstable manifolds of the NHIM enclose volumes of the energy surface that contain all reactive trajectories.

We have shown that these phase space structures can be realized in the neighborhood of the saddle using a Poincaré-Birkhoff normalization procedure. This procedure allows us to *unfold the dynamics* close to the equilibrium point and results in *explicit formulas* for the various phase space objects that govern the reaction, in ''normal form coordinates.'' These structures may then be mapped back into the original coordinate system. We have described the local geometry and dynamics and have illustrated this in considerable detail for the three DOF case. We demonstrated this technique by calculating a normal form for the HCN isomerization. The normal form was used to calculate the various local structures for this system and was shown to be of exceptionally high quality. As this paper demonstrates, this unfolding of the local dynamics enables us to engineer trajectories of any allowable type and also enables us to map trajectories explicitly through the region of validity of the normal form: we can take the point at which a trajectory enters such a local region and map it analytically to the point at which it will leave.

We have shown how global objects, such as the stable and unstable manifolds of the NHIM, may be constructed by continuing their local counterparts numerically outside of the neighborhood of the saddle, by integrating the equations of motion of the original system. The normal form is thus used to provide extremely accurate initial conditions for this globalization procedure, which then delivers a high-quality dynamical roadmap of the energy surface for the original system.

We define a new *dynamical reaction path in phase space* as the center curve of the volume of reactive trajectories enclosed by the stable and unstable manifolds of the NHIM, and have constructed such reaction paths for HCN isomerization. When projected into configuration space, these reaction paths differ from the usual minimum energy path that joins the relevant potential minima via the saddle and reveal a weakness in the use of the minimum energy path to characterize the reaction: a surface of section taken in the ''bottom'' of the HCN well shows that most reacting trajectories *avoid* the region around the conventional minimum energy path. In contrast, examining the surface of section at our dynamical reaction path reveals that it captures many more reacting trajectories. In particular, as we will mention later, these results call into question certain assumptions often made in the literature, e.g., ergodicity of the dynamics.

This paper also shows how quantum mechanics, at least in a semiclassical form, fits into our picture. In particular, it demonstrates how to construct complex tunnelling paths that connect both nonreacting and reacting trajectories, and provides a description of their structure. By incorporating tunnelling paths between *both* nonreacting and reacting trajectories, we have shown how one can compute a uniform transmission probability that is valid both above and below the saddle and have given an expression for the quantum mechanical flux in terms of the number of open transmission channels for a suitably computed normal form. The complex tunnelling paths, with the action integrals that we define, give the nonlinear tunneling corrections to this flux quantization, to any desired order, in a way which takes into account the full *dynamics*.

We described in detail how the local unfolding of the dynamics also elucidates the internal structure of the NHIM and its stable and unstable manifolds. By making use of this structure, we have provided an algorithm for computing homoclinic orbits connecting a NHIM, and heteroclinic orbits connecting two different NHIMs. Although such orbits have so far received essentially no attention in the molecular dynamics community, they are nevertheless of considerable importance for the study of reaction dynamics: as we explain, the heteroclinic connections that we compute form the *skeleton for rare events in phase space; they provide a mechanism for trajectories to pass through a succession of dividing surfaces* in multistage reactions involving several saddle-center-...-center equilibria. Together with our construction of homoclinic connections, the existence of multiple hetero-

clinic connections between different NHIMs provides both (1) a qualitative proof that *global* recrossing of any single dividing surface is an *inherent property of the dynamics* for many systems and (2) a *quantitative* tool for constructing (explicitly) the mechanisms underlying such global recrossings. At the same time, we show that the existence of certain special types of homoclinic connections (namely, those that connect a particular torus in a single NHIM to itself) are the ''signatures'' of a new type of high-dimensional *chaotic saddle*.[53] It is likely that such saddles play an important role for the consequences of chaos in reaction dynamics. Undoubtedly, there are many important implications in molecular dynamics for all of these orbits that beg for further study.

We cannot emphasize enough that it is essential that our study of dynamics is carried out in phase space. The phase space theory developed in this paper contains the complete information about the nonlinear dynamics. As we demonstrate, for example, by studying the projections of our dividing surface and NHIM into configuration space, such information cannot be obtained from conventional approaches which are based solely on a configuration space picture.

The theory that we present here opens many avenues for further research. We now outline some of these areas.

The construction of a dividing surface which has the bottleneck property and has no local recrossings, as explained in Sec. II B, relies on the existence of the NHIM. As in the case of two DOF, where the NHIM is a periodic orbit, the NHIM may in general undergo a bifurcation for energies high enough above the saddle energy.[64] This will lead to the ''breakdown'' of the validity of transition state theory, in the sense of not being able to construct a surface of no return separating reactants from products. Looking at it another way, the dynamics on the energy surface changes in such a way that the distinction between reactants and products becomes unclear. There have been numerous studies in the chemistry literature concerned with the breakdown, or validity, of transition state theory (e.g., Refs. 65–68). The bifurcations of NHIMs in the three DOF and general DOF cases, about which little is known, provides a fruitful subject for future studies.

Concerning quantum effects, a study of the localization of wave functions on the NHIM is relevant for transition state spectroscopy. The quantum normal form, together with the theory which we describe, provides a framework for such studies.

The stable and unstable manifolds of the NHIM provide the means to study global questions such as the location of reactive initial conditions far away from the transition region and violations of statistical assumptions about the global dynamics. The assumption that trajectories explore the energy surface ergodically typically underlies statistical rate theory. This assumption is not only the basis for the computation of statistical reaction rates but moreover for many sampling techniques that are used to obtain reactive trajectories. Such sampling techniques are called into question by the result of this paper that, *generically*, the dynamics near a saddle is integrable. The theory presented here offers the means to study nonstatistical effects on reaction rates: The reactive volumes bounded by the stable and unstable manifolds of the NHIMs tell us exactly which trajectories to ''sample'' for a given reaction. In a forthcoming paper,[57] we will show how the stable and unstable manifolds can be used to estimate the volume of the energy surface which contains the initial conditions for reactive trajectories. As we will show, for HCN this volume is significantly smaller than the total energy surface volume, which demonstrates that the assumption of ergodicity for this system is violated.

Although the studies in this paper call into question the automatic invocation of assumptions routinely made in molecular dynamics, at the same time we provide methods that enable one to understand and quantify the phase space dynamics of reactions without making such assumptions. Combining this approach with molecular dynamics methods should provide an interesting and fertile arena for future research.

ACKNOWLEDGMENTS

This research was supported by ONR Grant No. N00014-01-1-0769. H.W. acknowledges support by the Deutsche Forschungsgemeinschaft Grant No. Wa 1590/1-1.

[1] D. G. Truhlar, Faraday Discuss. **110**, 91 (1998).
[2] R. A. Marcus, Science **256**, 1523 (1992).
[3] J. C. Polanyi and A. H. Zewail, Acc. Chem. Res. **28**, 119 (1995).
[4] S. Wiggins, Physica D **44**, 471 (1990).
[5] S. Wiggins, *Chaotic Transport in Dynamical Systems* (Springer, Berlin, 1992).
[6] S. Wiggins, L. Wiesenfeld, C. Jaffé, and T. Uzer, Phys. Rev. Lett. **86**, 5478 (2001).
[7] T. Uzer, C. Jaffé, J. Palaciàn, P. Yanguas, and S. Wiggins, Nonlinearity **15**, 957 (2002).
[8] H. Waalkens and S. Wiggins, J. Phys. A **37**, L435 (2004).
[9] E. Wigner, Trans. Faraday Soc. **34**, 29 (1938).
[10] J. C. Keck, Adv. Chem. Phys. **13**, 85 (1967).
[11] D. G. Truhlar and B. C. Garrett, Annu. Rev. Phys. Chem. **35**, 159 (1984).
[12] S. Wiggins, *Normally Hyperbolic Invariant Manifolds in Dynamical Systems* (Springer, Berlin, 1994).
[13] H. Eyring, J. Chem. Phys. **3**, 107 (1934).
[14] W. H. Miller, J. Phys. Chem. A **102**, 793 (1998).
[15] P. Pechukas, Annu. Rev. Phys. Chem. **32**, 159 (1981).
[16] F. F. Crim, Acc. Chem. Res. **32**, 877 (1999).
[17] W. F. Polik, D. R. Guyer, and C. B. Moore, J. Chem. Phys. **92**, 3453 (1990).
[18] S. Shi and H. Rabitz, Comput. Phys. Commun. **63**, 71 (1991).
[19] S. P. Shah and S. A. Rice, J. Chem. Phys. **113**, 6536 (2000).
[20] C. Dellago, P. G. Bolhuis, F. S. Csajka, and D. Chandler, in *Classical and Quantum Dynamics in Condensed Phase Simulations*, edited by B. J. Berne, G. Ciccotti, and D. F. Coker (World Scientific, Singapore, 1998), pp. 51–66.
[21] G. Jacucci, M. Toller, G. DeLorenzi, and C. P. Flynn, Phys. Rev. Lett. **52**, 295 (1984).
[22] D. J. Wales, Science **293**, 2067 (2001).
[23] H. P. de Oliveira, A. M. Ozorio de Almeida, I. Damião Soares, and E. V. Tonini, Phys. Rev. D **65**, 083511 (2002).
[24] B. C. Hathorn and R. A. Marcus, J. Chem. Phys. **113**, 9497 (2000).
[25] B. C. Hathorn and R. A. Marcus, J. Chem. Phys. **111**, 4087 (1999).
[26] R. Siebert, R. Schinke, and M. Bittererova, Phys. Chem. Chem. Phys. **3**, 1795 (2001).
[27] C. Jaffé, S. D. Ross, M. W. Lo, J. Marsden, D. Farrelly, and T. Uzer, Phys. Rev. Lett. **89**, 011101 (2002).
[28] P. Pechukas and F. J. McLafferty, J. Chem. Phys. **58**, 1622 (1973).
[29] P. Pechukas and E. Pollak, J. Chem. Phys. **69**, 1218 (1978).
[30] L. Sun, K. Song, and W. L. Hase, Science **296**, 875 (2002).
[31] S. C. Ammal, H. Yamataka, M. Aida, and M. Dupuis, Science **299**, 1555 (2003).
[32] R. J. Hinde and R. S. Berry, J. Chem. Phys. **99**, 2942 (1993).
[33] T. Komatsuzaki and R. S. Berry, J. Chem. Phys. **110**, 9160 (1999).

[34] W. H. Miller, Faraday Discuss. **62**, 40 (1977).
[35] R. Hernandez and W. H. Miller, Chem. Phys. Lett. **214**, 129 (1993).
[36] G. D. Birkhoff, *Dynamical Systems* (American Mathematical Society, Providence, RI, 1927).
[37] F. Gustavson, Astron. J. **71**, 670 (1966).
[38] H. Rüssmann, Math. Ann. **154**, 285 (1964).
[39] C. L. Siegel, Math. Ann. **128**, 144 (1954).
[40] V. I. Arnol'd, V. V. Kozlov, and A. I. Neishtadt, in *Dynamical Systems III*, Encyclopaedia of Mathematical Sciences, edited by V. I. Arnol'd, Vol. 3 (Springer, Berlin, 1988).
[41] M. Ali, J. Math. Phys. **26**, 2565 (1985).
[42] B. Eckhardt, J. Phys. A **19**, 2961 (1986).
[43] J. H. Van Vleck, Rev. Mod. Phys. **23**, 213 (1951).
[44] P. Crehan, J. Phys. A **23**, 5815 (1990).
[45] M. J. Cohen, N. C. Handy, R. Hernandez, and W. H. Miller, Chem. Phys. Lett. **192**, 407 (1992).
[46] R. Hernandez, J. Chem. Phys. **101**, 9534 (1994).
[47] S. C. Creagh, Nonlinearity **17**, 1261 (2004).
[48] M. V. Berry and K. E. Mount, Rep. Prog. Phys. **35**, 315 (1972).
[49] E. R. Lovejoy and C. B. Moore, J. Chem. Phys. **98**, 7846 (1993).
[50] B. J. van Wees, H. van Houten, C. W. J. Beenakker, J. G. Williamson, L. P. Kouwenhoven, D. van der Marel, and C. T. Foxen, Phys. Rev. Lett. **60**, 848 (1988).
[51] L. M. Krans, J. M. van Ruitenbeek, V. V. Fisun, L. K. Yanson, and L. J. de Jongh, Nature (London) **375**, 767 (1995).
[52] J. N. Murrell, S. Carter, and L. O. Halonen, J. Mol. Spectrosc. **93**, 307 (1982).
[53] H. Waalkens, A. Burbanks, and S. Wiggins, J. Phys. A **37**, L257 (2004).
[54] J. I. Steinfeld, J. S. Francisco, and W. L. Hase, *Chemical Kinetics and Dynamics* (Prentice-Hall, New Jersey, 1989).
[55] N. De Leon, M. A. Mehta, and R. Q. Topper, J. Chem. Phys. **94**, 8310 (1991); **94**, 8329 (1991).
[56] A. M. O. de Almeida, N. De Leon, M. A. Mehta, and C. C. Marston, Physica D **46**, 265 (1990).
[57] H. Waalkens, A. Burbanks, and S. Wiggins (unpublished).
[58] W. E, W. Ren, and E. Vanden-Eijnden, J. Appl. Phys. **93**, 2275 (2003).
[59] See the Chaos Focus issue on "Chaotic Scattering", **3** (1997).
[60] Y.-C. Lai and R. L. Winslow, Phys. Rev. Lett. **74**, 5208 (1995).
[61] H. E. Nusse and J. A. Yorke, Physica D **36**, 137 (1989).
[62] J. Cresson, J. Diff. Eqns. **187**, 269 (2003).
[63] J. C. Schön, M. A. C. Wevers, and M. Jansen, J. Phys.: Condens. Matter **15**, 5479 (2003).
[64] E. Pollak, M. S. Child, and P. Pechukas, J. Chem. Phys. **72**, 1669 (1980).
[65] E. K. Grimmelmann and L. L. Lohr, Jr., Chem. Phys. Lett. **48**, 487 (1977).
[66] S. Chapman, S. M. Hornstein, and W. H. Miller, J. Am. Ceram. Soc. **97**, 892 (1975).
[67] D. I. Sverdlik and G. W. Koeppl, Chem. Phys. Lett. **59**, 449 (1978).
[68] W. J. Chesnavich, Chem. Phys. Lett. **53**, 300 (1978).